

Review

# Austenite-Based Fe-Mn-Al-C Lightweight Steels: Research and Prospective

Hua Ding <sup>1,2,\*</sup>, Degang Liu <sup>3,\*</sup>, Minghui Cai <sup>1,2</sup> and Yu Zhang <sup>1,2</sup>

<sup>1</sup> School of Materials Science and Engineering, Northeastern University, Shenyang 110819, China

<sup>2</sup> Key Lab of Lightweight Structural Materials, Northeastern University, Shenyang 110819, China

<sup>3</sup> School of Mechanical Engineering, Shandong University of Technology, Zibo 255049, China

\* Correspondence: dingh@smm.neu.edu.cn (H.D.); liudegang@sdu.edu.cn (D.L.)

**Abstract:** Fe-Mn-Al-C lightweight steels have been investigated intensely in the last a few years. There are basically four types of Fe-Mn-Al-C steels, ferritic, ferrite-based duplex/triplex (ferrite + austenite, ferrite + austenite + martensite), austenite-based duplex (ferrite + austenite), and single-austenitic. Among these steels, austenite-based lightweight steels generally exhibit high strength, good ductility, and outstanding weight reduction effects. Due to the addition of Al and high C content,  $\kappa'$ -carbide and  $\kappa$ -carbide are prone to form in the austenite grain interior and at grain boundaries of lightweight steels, respectively, and play critical roles in controlling the microstructures and mechanical properties of the steels. The microstructural evolution, strengthening mechanisms, and deformation behaviors of these lightweight steels are quite different from those of the mild conventional steels and TRIP/TWIP steels due to their high stacking fault energies. The relationship between the microstructures and mechanical properties has been widely investigated, and several deformation mechanisms have also been proposed for austenite-based lightweight steels. In this paper, the current research works are reviewed and the prospectives of the austenite-based Fe-Mn-Al-C lightweight steels are discussed.

**Keywords:** Fe-Mn-Al-C lightweight steel;  $\kappa'$ / $\kappa$ -carbide; microstructure; mechanical property; deformation mechanism



**Citation:** Ding, H.; Liu, D.; Cai, M.; Zhang, Y. Austenite-Based Fe-Mn-Al-C Lightweight Steels: Research and Prospective. *Metals* **2022**, *12*, 1572. <https://doi.org/10.3390/met12101572>

Academic Editor: Juan Wang

Received: 23 August 2022

Accepted: 18 September 2022

Published: 22 September 2022

**Publisher's Note:** MDPI stays neutral with regard to jurisdictional claims in published maps and institutional affiliations.



**Copyright:** © 2022 by the authors. Licensee MDPI, Basel, Switzerland. This article is an open access article distributed under the terms and conditions of the Creative Commons Attribution (CC BY) license (<https://creativecommons.org/licenses/by/4.0/>).

## 1. Introduction

Fe-Mn-Al-C lightweight steels, also known as low-density steels, first developed in the 1950s as substitutes of Fe-Cr-Ni stainless steels, have drawn research interests for their good comprehensive mechanical properties and lightweight effect as structural materials in the last a few years [1]. Fe-Mn-Al-C lightweight steels possess a variety of mechanical properties ranging by tailoring their microstructures, e.g., yield strength of 300–1200 MPa, ultimate tensile strength of 600–1500 MPa and total elongation of 30–100% [1]. In addition, these alloys have been reported to possess good service properties such as fatigue properties [2–7] and oxidation resistance at elevated temperatures [8–12]. These promising properties of Fe-Mn-Al-C steels have attracted considerable interests in several fields, such as transportation, especially in automobile vehicles and power trains as well as military use [1].

Based on the phase constituents of the materials, several types of Fe-Mn-Al-C steels have been investigated, such as ferritic, ferrite-based duplex/triplex (ferrite + austenite, ferrite + austenite + martensite), austenite-based duplex (ferrite + austenite), and austenitic ones.

Fe-Al lightweight steels alloyed with Mn lower than 5% and a very low C content possess a fully ferritic microstructure, which may contain A2-disordered FeAl, B2-ordered FeAl (Figure 1a) and DO<sub>3</sub>-ordered Fe<sub>3</sub>Al (Figure 1b) at room temperature depending on Al content [1,13–20]. The Fe-Al alloys based on FeAl or Fe<sub>3</sub>Al intermetallic compounds always show promising properties for high temperature structural applications due to their resistance to oxidation, sulfidation and carburizing, good resistance to corrosion

in sea water, high resistance to wear, erosion, or cavitation, and high strength-to-weight ratios [19,20].

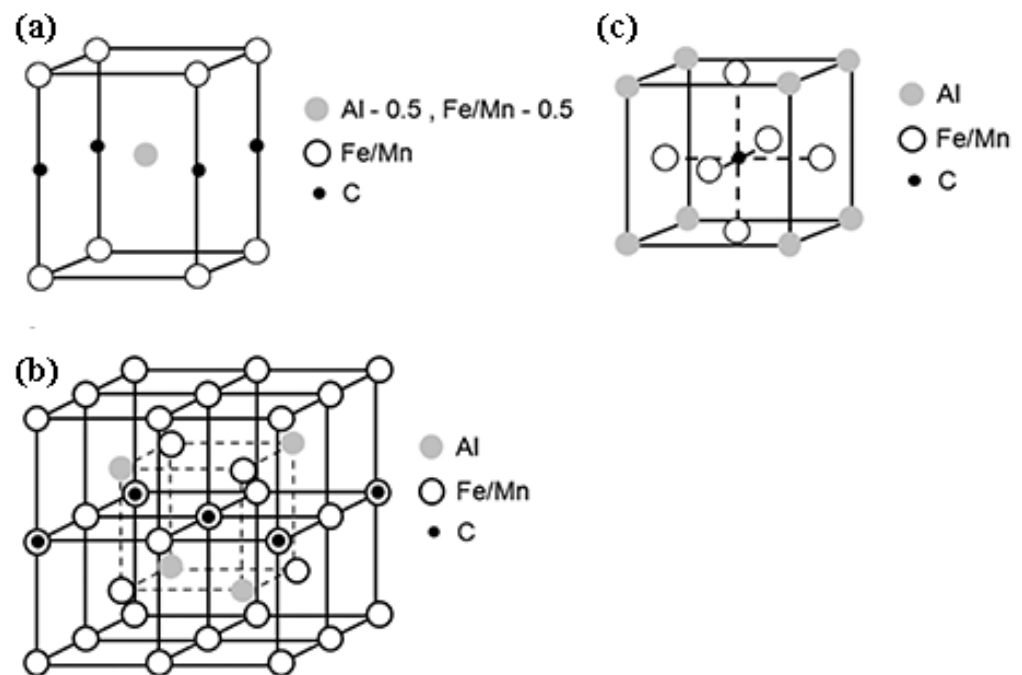


**Figure 1.** Schematic visualization [18] of the supercell of (a) B2, (b) D0<sub>3</sub>, (c)  $\kappa'$ -carbide. (Reproduced with permission from [18]. Copyright 2013 Elsevier).

Ferrite-based duplex and triplex Fe-Mn-Al-C steels with moderate Mn (Mn: 2–12%) and C contents (C: 0.05–0.5%) possess the microstructures consisting of austenite +  $\delta/\alpha$ -ferrite and austenite +  $\delta/\alpha$ -ferrite + martensite, respectively, in which the fraction of ferrite is higher than 50% [21–37]. In this kind of steels, the transformation-induced plasticity (TRIP) effect is a very important mechanism in enhancing the strength and ductility of the materials.

Austenite-based duplex Fe-Mn-Al-C steels containing a higher Mn content, typically between 8 and 32%, Al up to 12%, and C between 0.3 and 1.2% are characterized by austenite +  $\delta/\alpha$ -ferrite or austenite +  $\alpha$ -ferrite [18,38–84]. Different from the ferrite-duplex one, the fraction of austenite is more than half in the austenite-based duplex steels, and the stability of austenite is quite high due to the high alloying elements.

Full austenite structure at room temperature can be obtained in Fe-Mn-Al-C steels with high Mn and high C contents, which are in the range of 13–40% and 0.6–2.0%, respectively, in spite of the high-Al content [63,64,85–130]. Meanwhile, the fully austenitic microstructure has been also obtained in the medium-Mn Fe-Mn-Al-C steels [46].

The increase in Al content in steels exhibits good lightweight effects but also easily gives a rise to cause the formation of brittle intermetallic compounds, eventually leading to poor ductility [131]. Among these four types of lightweight steels mentioned above, the austenite-based Fe-Mn-Al-C steels show superior weight reduction effect via alloying more Al and possess both high strength and ductility, which are closely associated with their unique microstructure features and deformation mechanisms. The microstructural evolution of austenite-based Fe-Mn-Al-C steels is different from the conventional steels, and they also show distinguished features from TRIP and TWIP steels due to the additions of relatively high alloying elements. The physical metallurgy is quite complex and there are still some theoretical aspects which needs to be clarified in the austenite-based Fe-Mn-Al-C lightweight steels. Furthermore, the detailed research work needs to be carried out for practical applications. In this paper, the recent developments of austenite-based single and

duplex Fe-Mn-Al-C lightweight steels are reviewed and future directions for the research in Fe-Mn-Al-C steels are proposed.

## 2. Phase Constituents in the Austenite-Based Fe-Mn-Al-C Lightweight Steels

The medium-Mn ( $5\% \leq \text{Mn} \leq 12\%$ ) and high-Mn ( $\text{Mn} > 12\%$ ) lightweight steels are characterized by single austenite and austenite-based duplex (austenite + ferrite) matrix due to their high content of austenite stabilizer elements of Mn and C [129]. When the content of ferrite stabilizer element, i.e., Al, is high and the associated  $\text{Ni}_{\text{eq}}/\text{Cr}_{\text{eq}}$  is relatively low, a considerable amount of banded coarse  $\delta$ -ferrite forms during solidification and became inherited during subsequent hot rolling, cold rolling and annealing [44,80,81,129,132–134]. Meanwhile, some fine  $\alpha$ -ferrite grains could form during hot deformation or annealing in the intercritical temperature ( $\gamma \rightarrow \alpha$ ), which is propitious to the microstructure refinement [46,81,111].

Regarding precipitation, the formation of  $\kappa'$ -carbide precipitates depends on heat treatment conditions. The phase has a perovskite crystal structure designated as  $L'1_2$ , and its ideal stoichiometry is  $(\text{Fe}, \text{Mn})_3\text{AlC}$  [1,135]. The crystal structure of the phase is illustrated in Figure 1c. A metastable  $(\text{Fe}, \text{Mn})_3\text{AlC}_x$  ( $x < 1$ ) phase has the same crystal structure as the phase but with an uncompleted occupation of the C atoms [136]. The off-stoichiometric concentration of Al was explained by mismatch-induced strain, which facilitates the occupation of Al sites in the  $\kappa'$ -carbide by Mn atoms [123,125,136].

When the high-Mn austenitic lightweight steels were quenched from high temperature or aged at 450–650 °C, nano-sized  $\kappa'$ -carbide particles formed within austenite grains [90,91,116,125]. This intra-granular  $\kappa'$ -carbide is a metastable  $(\text{Fe}, \text{Mn})_3\text{AlC}_x$  phase which is coherent to the matrix. The steel matrix (austenite) and  $\kappa'$  phase have the cube-on-cube crystallographic orientation relationship from these selected area diffraction patterns (SADPs), i.e.,  $[100]_{\kappa} // [100]_{\gamma}$ ,  $(100)_{\kappa} // (100)_{\gamma}$  [114]. It has been long believed that the formation of intra-granular  $\kappa'$ -carbide is through spinodal decomposition and following ordering reaction [137,138]. Transmission electron microscopy and X-ray diffraction were generally used to provide experimental evidence supporting the spinodal decomposition-ordering mechanism by observing the modulated structure [139], diffuse satellites around the (200) diffraction spots in electron diffraction patterns, and XRD side band peaks around the (200) reflections [138,140]. However, some recent transmission electron microscopy (TEM, FEI Titan Themis, Hillsboro, OR, USA) and atomic probe tomography (APT, FEI Helios Nano-Lab 600i, Hillsboro, OR, USA) results obtained in an Fe-30Mn-9Al-1.2C lightweight steel indicated that the formation of an ordered structure was earlier than chemical partitioning of any solute elements during the early stage of  $\kappa'$ -carbide precipitation [141]. Near-atomic scale characterization of an austenite-based Fe-20Mn-9Al-3Cr-1.2C steel, using high-resolution scanning TEM (HRSTEM, FEI Tecnai G2-20, Hillsboro, OR, USA) and APT also revealed that the initially-formed  $\kappa'$ -carbide (2–3 nm in particle size) are characterized by an ordered  $L'1_2$  structure but without detectable chemical partitioning [114]. However, the increasing Mn content could delay the formation of intra-granular  $\kappa'$ -carbide via suppressing the C occupation of the vacancy at the body-centered site of  $L'1_2$ , which is related to the C ordering process [123,125,136]. Thus, the intra-granular  $\kappa'$ -carbide is more prone to precipitate in medium-Mn lightweight steels.

Meanwhile, the extended aging and relative-low-temperature annealing caused the precipitation of perovskite-structured  $(\text{Fe}, \text{Mn})_3\text{AlC}_x$  carbide at the grain boundaries of austenite [40–42,45,57,58,62,90,91,99,119]. Hereafter, we distinguish the ordered grain boundary  $L'1_2$  phase from the intra-granular  $\kappa'$  phase of the same structure by naming the former as  $\kappa$ -carbide. Such inter-granular  $\kappa$ -carbide grew into the austenite grains in the form of a lamellar structure together with  $\alpha$ -ferrite through the following dominant route: the eutectoid reaction  $\gamma \rightarrow \kappa + \alpha$  [40]. The cellular transformation is a form of continuous reaction which occurs during the transformation of high-temperature austenite into lamellae of austenite,  $\alpha$ -ferrite, and  $\kappa$ -carbide [62]. The formation of coarse second-phase particles

which have a lamellar morphology was also observed after aging for a longer period of time in a solution treated Fe-(11–30)Mn-(7.8–10)Al-(0.8–2.0)C alloys [45,58,90,91,99,119].

In the Fe-27Mn-12Al-0.8C duplex lightweight steel [18], various ordered phases such as DO<sub>3</sub>, B2 and  $\kappa'$ -carbide were formed in the duplex microstructure upon quenching in water after intercritical annealing. Fine DO<sub>3</sub> were evenly distributed through both B2 domains and disordered ferrite matrix. Meanwhile, nano-sized  $\kappa'$ -carbides precipitated in austenite. Similar results were also attained in the Fe-11Mn-10Al-0.9/1.2C, Fe-15Mn-10Al-1.0C and Fe-18Mn-10Al-1.2C steels alloyed with lower Mn contents [46,59,63].

Since there are variations of phase constituents in Fe-Mn-Al-C steels which are controlled by compositions and processing schedules, the mechanical behavior could be tailored in a wide range for these kinds of steels.

### 3. Mechanical Properties

The mechanical properties of the representative medium-Mn [38,40–42,45,46,50,51,53–55,84] and high-Mn [3,18,57,58,63,67,69,78,79,83,85,91,100,103,107,109–111,113,116,122,124,127,129,141–159] lightweight steels are shown in Figure 2a,b. It is clearly indicated that both the medium-Mn and high-Mn steels possess good mechanical properties and show large space to be regulated, yield strength: 375–1850 MPa, ultimate tensile strength: 765–1978 MPa, and total elongation: 1–80%. Generally, both intra-granular  $\kappa'$ -carbide and inter-granular one can effectively improve the yield strength of lightweight steels, regardless of Mn content [40–42,45,46,57,58,84,85,91,122]. However, the coarse inter-granular  $\kappa$ -carbide results in an abrupt loss of elongation, while the fine intra-granular  $\kappa'$ -carbide enhance the strengths of lightweight steels without significantly sacrificing ductility but brings out a relatively high yield ratio (>0.9) [40–42,45,46,91]. Moreover, although the relationship between strength and ductility of duplex and single-austenitic lightweight steels follow the “banana” curve, the mechanical properties of single-austenitic steels with high-Mn content seems to be superior to those of duplex ones. For instance, the austenitic steel (Fe-28Mn-9Al-1.8C) demonstrates ultrahigh strength (yield strength of 1383 MPa and ultimate tensile strength of 1487 MPa) with good elongation of ~32.5% [91]. The increase in Mn content seems to bring more room for improving the strength and ductility of steels, but it also increases the difficulty in fabrication, not to mention the sharp increment in material cost [160]. Achieving high performance lightweight steel and maintaining its economy is also an important subject during its development process.

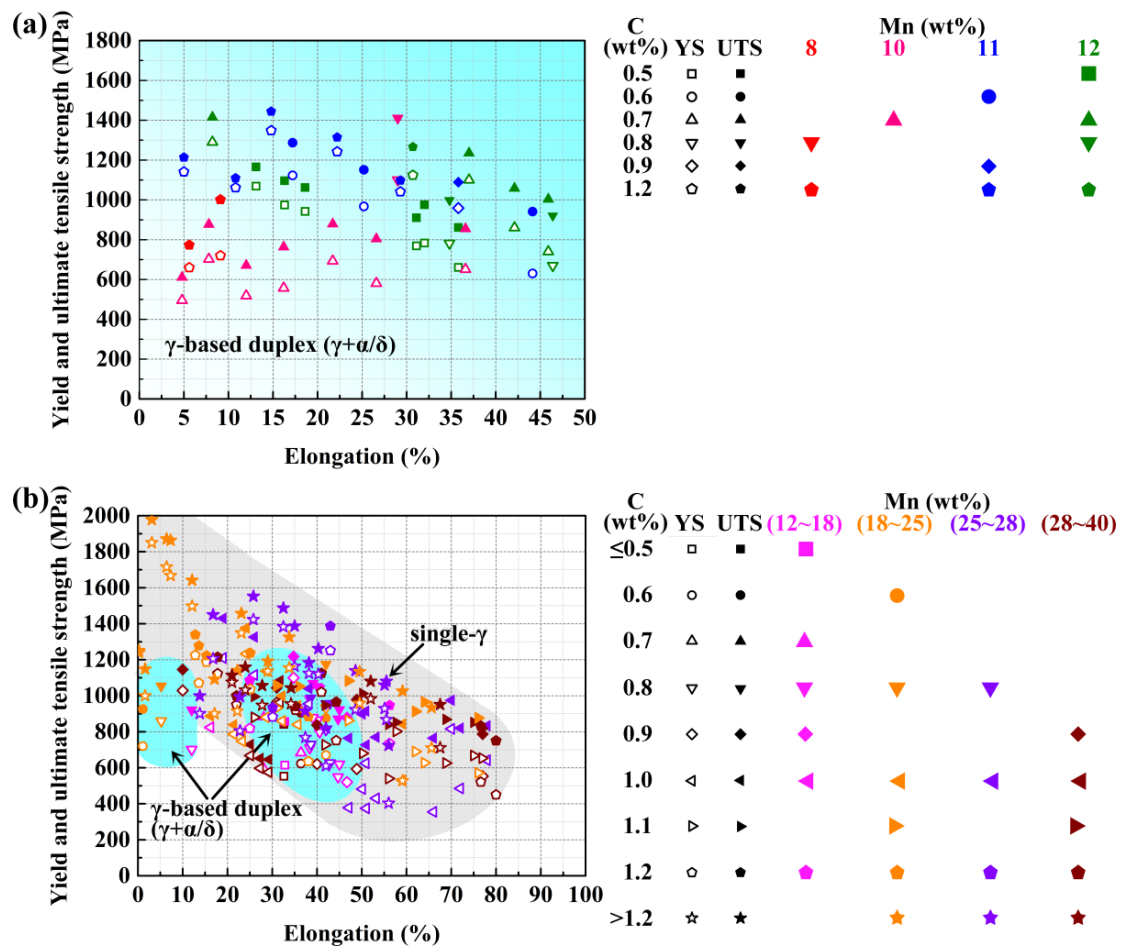


**Figure 2.** Comparison of room-temperature tensile properties of the present developed (a) medium-Mn [10,38,40–42,45,46,50,51,53–55,84] and (b) high-Mn [3,18,57,58,63,67,69,78,79,83,85,91,100,103,107,109–111,113,116,122,124,127,129,141,143–159] lightweight steels.

#### 4. Strengthening Mechanisms

Solid solution hardening plays a role in the strengthening of Fe-Mn-Al-C steels due to the high amount of alloying elements C, Al, and Mn in these steels and grain refinement is another strengthening mechanism [46,74,125,141]. The austenite grain size can be refined by thermomechanical processing (TMP) combined with cold working and annealing [42,111,155]. The existence of ferrite can also make the austenite size decrease owing to the prohibition of growth of austenite in both medium-Mn and high-Mn lightweight steels [46,111].

It was reported that the yield strength of these steels increases as the Al concentration increases [74]. The high yield strength of 12Al steel, 952 MPa, is due to fine grain strengthening, precipitation strengthening, the existence of ferrite, and Al solution strengthening. Quantitative investigations in Fe-26Mn-Al-1C indicated that the effect of Al on yield strength of the alloys is not quite significant in the Al range of 3 to 10%. Precipitation hardening is the most significant strengthening mechanism in the alloys containing homogeneously distributed nano-sized  $\kappa'$ -carbides.

Dislocations moving through an austenitic matrix containing intra-granular  $\kappa'$ -carbide can either shear the precipitates or bypass them and consequently result in alloy strengthening [116]. In Fe-Mn-Al-C lightweight steels, it is believed that the operative mechanism (shearing mechanism or Orowan bypassing mechanism) and the corresponding strengthening effect are closely associated with the size of  $\kappa'$ -carbide [116,125]. For a given volume fraction (~20%), Yao et al. calculated the shearing strengthening effect of the Fe-30.4Mn-

8Al-1.2C steel aged at 600 °C for 24 h based on the antiphase boundary (APB) energy, which is about 500 MPa [116]. As the size of  $\kappa'$ -carbide is beyond the critical radius (~6.8 to 13.5 nm), the Orowan looping can in principle be activated [116]. Since the lower Mn content facilitates the formation of intra-granular  $\kappa'$ -carbide [123,125,136], the precipitation hardening is expected to reach the higher value in the medium-Mn steels. Liu et al. studied the strengthening mechanisms of the cold-rolled Fe-11Mn-xAl-yC ( $x = 7/11$ ,  $y = 0.6/0.9/1.2$ ) medium-Mn lightweight steels annealed at 700–1100 °C; see Figure 3 [46]. It is clearly observed that the maximum of the  $\kappa'$ -carbide precipitation strengthening effect of the 1000 °C-annealed Fe-11Mn-10Al-1.2C steel is estimated as 679 MPa. Meanwhile, the existence of high density dislocations in the partially-recrystallized hetero-structured Fe-11Mn-7Al-0.6C steels also results in a considerable increment in yield strength of the materials.

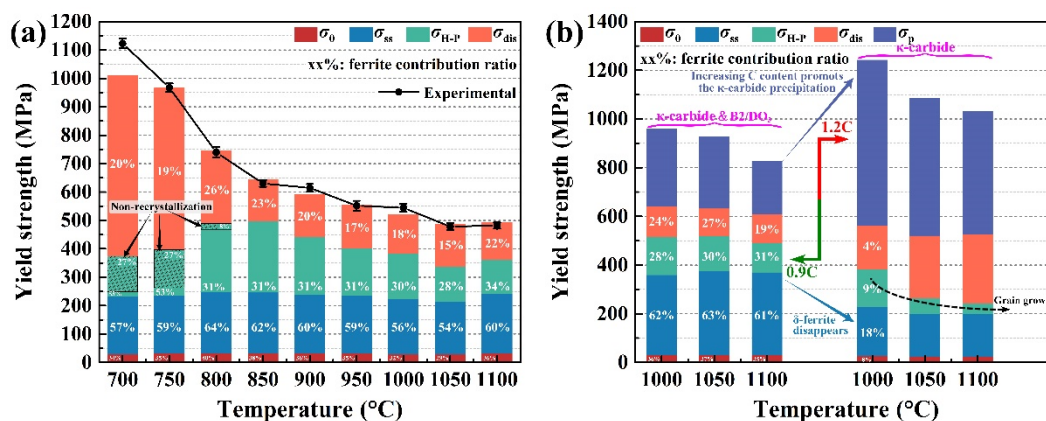


**Figure 3.** The calculated yield strength values for assessing the strengthening mechanisms of the (a) Fe-11Mn-7Al-0.6C steel and (b) Fe-11Mn-10Al-0.9/1.2C steels under various annealing temperatures [46]. (Reprinted with permission from [46]. Copyright 2022 Elsevier).

### 5. Strain Hardening Behaviors and Deformation Mechanisms

Several researchers investigated the strain hardening behaviors of Fe-Mn-Al-C steels. The results in the investigation of tensile deformation of a duplex Fe-20Mn-9Al-0.6C steel [67] revealed that strain hardening in both austenite and ferrite was monotonic during tensile deformation, but the strain hardening exponent of austenite was higher than that of ferrite, indicating the better strain hardenability of austenite. Three low-density Fe-18Mn-10Al-xC steels containing 0.5, 0.8 and 1.2 C (wt%) were utilized to investigate effects of C contents on the microstructural evolution and the corresponding mechanical behaviors during plastic deformation [63]. The differential Crussard–Jaoul (C–J) analysis demonstrated a two-stage strain hardening behavior in both 0.5C and 0.8C steels and a three-stage one in the 1.2C steel. This difference in strain hardening behavior was further understood in terms of microstructural analysis at the different stages of plastic deformation.

The strain hardening behavior in relation with the evolving dislocation substructures during uniaxial tensile deformation for an austenite-ferrite Fe-18.1Mn-9.6Al-0.65C steel was investigated [77]. The steel consisted of austenite and ferrite and possessed a good combination in mechanical properties. The deformation mode of austenite is dominated by planar glide and Taylor lattices and microbands formed as the deformation proceeded, whereas dislocation nodes, dislocation cells, and cell blocks formed due to the occurrence of wavy glide in ferrite, as shown in Figure 4 [77]. Three-stage strain hardening behavior was revealed in this steel, which is similar to the aforementioned steel. Since the increase of Al content in the steels increases the volume fraction of shearable  $\kappa'$ -carbide precipitates, an increased strain softening is activated in glide plane, which results in a decreased density of slip bands and significant decrease of the strain hardening rate [107]. Generally, the Fe-Mn-Al-C steels containing intra-granular  $\kappa'$ -carbides show low strain hardening rate because the nanocrystalline coherent precipitates are easily sheared by gliding dislocations [131].

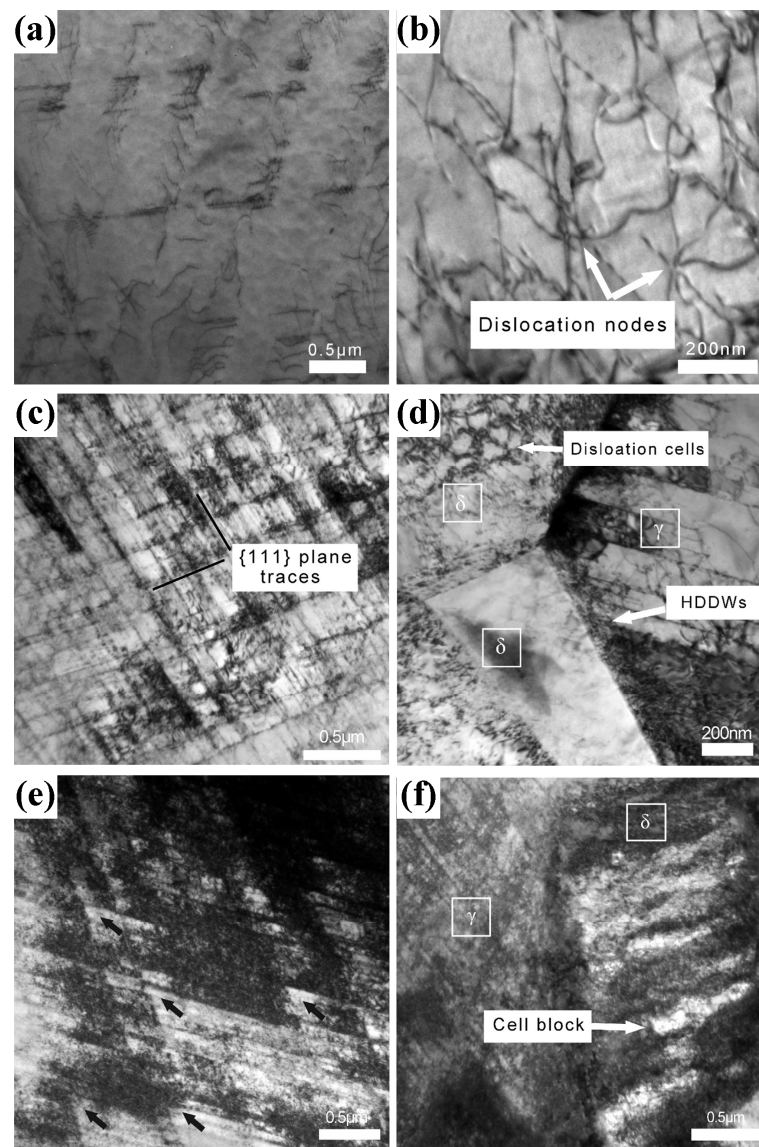


**Figure 4.** Dislocation substructure evolution within (a,c,e) austenite ( $\gamma$ ) and (b,d,f) ferrite ( $\delta$ ) in the Fe-18.1Mn-9.6Al-0.65C steel at different strains. (a,b)  $\epsilon = 0.02$ : (a) planar dislocation arrays, (b) dislocation nodes, (c) Taylor lattices ( $\epsilon = 0.18$ ), (d) dislocation cells ( $\epsilon = 0.10$ ), (e,f)  $\epsilon = 0.36$ : (e) microbands intersections, (f) cell block [77]. (Reproduced with permission from [77]. Copyright 2015 Elsevier).

The deformation mechanisms of austenite can be predicted basing on the thermodynamic calculation of stacking fault energy (SFE) [51,54,64,86,94]. It was reported that TRIP effect appears when the SFE is lower than  $\leq 18$  mJ/m<sup>2</sup>, and TWIP effect is dominant when the SFE is between 18–35 mJ/m<sup>2</sup>. When the SFE is higher than 60 mJ/m<sup>2</sup>, neither TRIP nor TWIP effect appears [161]. Mn, C and Al all increase the SFEs of Fe-Mn-Al-C steels. Generally, for FCC materials, it is difficult for extended partials to form when the material possesses high SFE. Therefore, cross slip of screw dislocations of the extended partials is easy and wavy slip would be dominant, forming cellular structure. However, planar slip features have been found in the FCC materials with high solute element concentrations. In this case, SFE is not the dominant factor influencing the deformation mode.

There are basically three deformation mechanisms reported in high SFE Fe-Mn-Al-C steels, shear band-induced plasticity (SIP) [75], microband-induced plasticity (MBIP) [87,89], and dynamic slip band refinement [97]; see Figure 5. For the SIP mechanism, it was suggested that the enhanced ductility is closely associated with the formation of the

homogeneous shear band accompanied by the dislocation glide sustained by the uniform arrangement of nano-size  $\kappa'$ -carbides coherent to the austenite matrix with defined inter-particle spacing. For the MBIP mechanism, planar slip occurs in austenite when the strain is low, Taylor lattice appear as the deformation proceeds and microbands form afterwards, increasing the strain hardening capacity of the steels. Strain hardening by dynamic slip band refinement in a Fe-30.4Mn-8Al-1.2C high-Mn lightweight steel was investigated, and it was characterized that material deforms mainly by planar dislocation slip causing the formation of slip bands [97]. The deformation mechanism was therefore regarded as dynamic slip band refinement. This slip band refinement-induced plasticity (SRIP) was also verified in Fe-29.8Mn-7.65Al-1.11C steel [122].

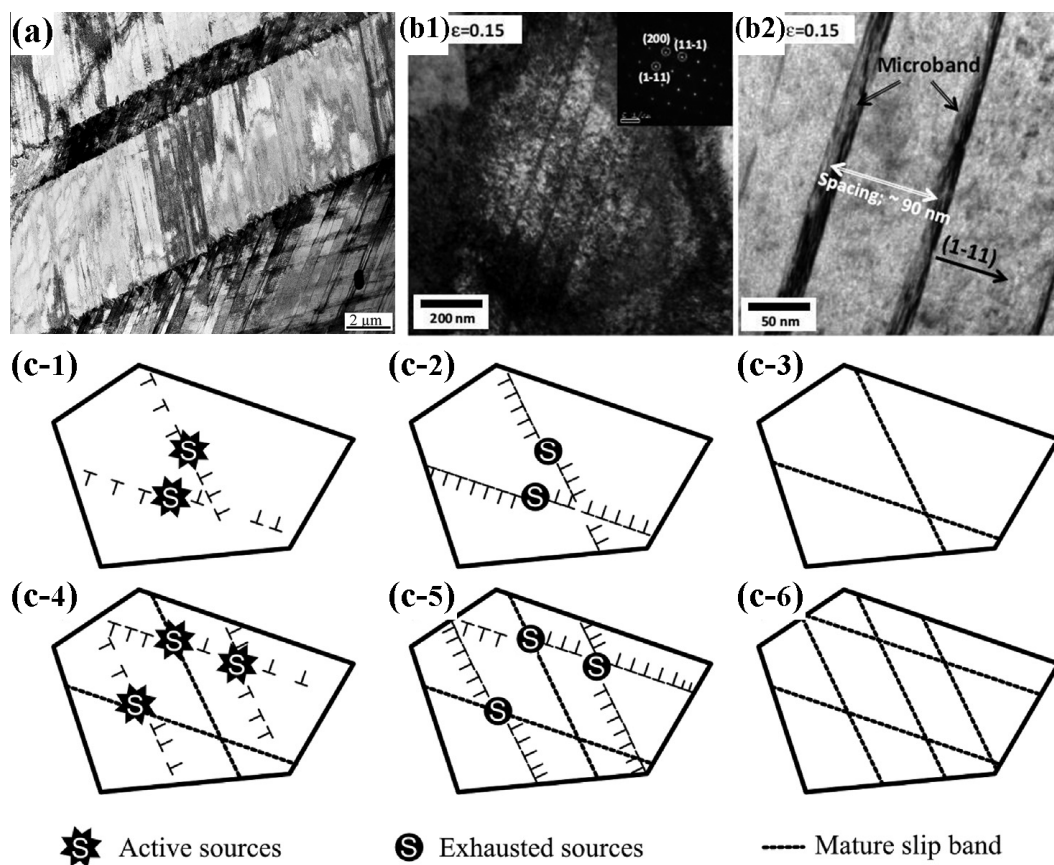


**Figure 5.** Three deformation mechanisms reported in high SFE Fe-Mn-Al-C steels. (a) shear band-induced plasticity: uniformly arranged shear bands on {111} planes within the austenitic matrix of a deformed high-Mn steel [75] (Reproduced with permission from [75]. Copyright 2016 Wiley.); (b) microband-induced plasticity: (b1) and (b2) well-developed microbands having distinct boundaries in austenite of the medium-Mn duplex lightweight steel at the true strain of 0.15 [51] (Reproduced with permission from [51]. Copyright 2015 Elsevier). (c) schematic illustration of dynamic slip band refinement: (c-1) activation of sources, (c-2) slip planes filled up with dislocations. (c-3) exhausted sources due to back stresses and fully developed slip bands, (c-4) activation of new sources, (c-5) and (c-6) newly activated sources undergone the same evolution as the previous sources leading to a refinement of the slip band substructure [97] (Reproduced with permission from [97]. Copyright 2016 Elsevier).

Tensile deformation of Fe-27Mn-12Al-0.8C duplex steel was studied in association with ordered phases [18]. In austenite, a single-planar dislocation glide is a dominant mechanism at low strains and multiple planar slip occurs at high strains, whereas short, straight segments of paired dislocations with narrow mechanical antiphase boundaries were formed in ferrite. It was reported that strain hardening of the duplex steel is associated

with the combined effect of the shearing of nano-sized ordered phase by superdislocations in ferrite and planar gliding dislocations in austenite.

## 6. Effect of Trace Alloying Elements

Kim et al. investigated the effect of another lightweight element, Si, on deformation mechanisms in light weight steels by atomic-scale analysis [120]. It was found that the addition of Si accelerated the formation kinetics of the  $\kappa'$  precipitates and increased the partitioning coefficient of carbon from 2.4 to 5.3. C-rich  $\kappa'$ -carbides are more resistant to shearing by dislocations due to a higher coherency strain and the formation of Al-C bonding which makes dislocation motion energetically more difficult. Therefore, the energy required for dislocation shearing  $\kappa'$ -carbides in the aged 1% Si steel was higher than the one in the aged Si-free steel.

The effect of Mo addition on the precipitation behavior the  $\kappa'$ -carbide in the austenitic Fe-Mn-Al-C lightweight steels was investigated [162]. First-principle calculations indicated that the substitution of Fe or Mn by Mo in  $\kappa'$ -carbide is energetically unfavorable with respect to the formation energy and it increases strain energy contribution to interfacial energy between austenite matrix and  $\kappa'$ -carbide. TEM observation and nano-indentation experiments showed that Mo delayed the kinetics of  $\kappa'$ -carbide formation and changed the age hardening behavior. This calculation was also verified by APT analysis, showing both are in a good agreement.

Sutou et al. reported the addition of Cr could improve the strength, hardness and cold-workability of Fe-20Mn-Al-C steels with higher C and Al contents [69]. The addition of Cr, which is a ferrite stabilizer, suppresses the formation of coarse inter-granular  $\kappa$ -carbides, and consequently, austenite retains more stability due to an increase in the amount of carbon inside austenite [163]. The increasing content of Cr in the Fe-20Mn-9Al-1.2C lightweight steel increased the volume fraction of ferrite but decreased the volume fraction of intra-granular  $\kappa'$ -carbide. Meanwhile, the increased Cr content also significantly slowed down the growth rate of  $\kappa'$ -carbides during isothermal aging treatment at 600 °C, as shown in Figure 6 [164].

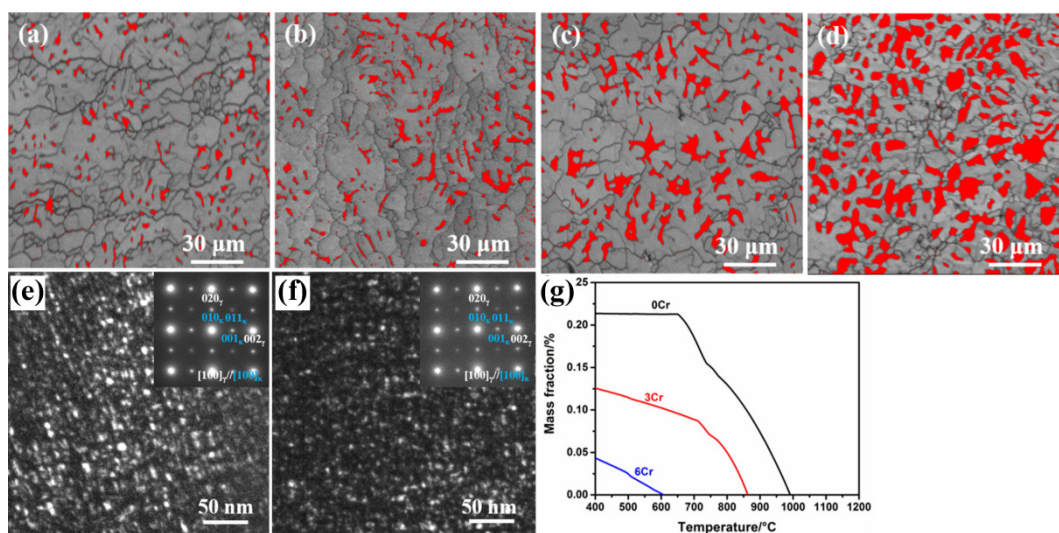


**Figure 6.** Electron backscattered diffraction (EBSD) phase maps of the as-cast Fe-20Mn-9Al-1.2C steels with different Cr content [164]: (a) 0Cr; (b) 3Cr; (c) 6Cr; and (d) 9Cr (red and gray contrasts indicate  $\delta$ -ferrite and  $\gamma$ -austenite phases, respectively). TEM DF images of  $\kappa'$ -carbides of the aged steels with (e) 0Cr and (f) 3Cr contents and (g) the thermodynamic calculation showing the variation in the mass fraction of  $\kappa'$ -carbides different Cr content. (Reproduced with permission from [164]. Copyright 2022 Elsevier).

V has been added in the austenite-based lightweight steel so as to improve the strength and strain hardening rate through dual-precipitation of V-carbides and  $\kappa'$ -carbide and the alloying element V could exert an impact on the precipitation behavior of  $\kappa'$ -carbide [152,156]. First principle analysis showed that the addition of V would increase the nucleation barrier energy of  $\kappa'$ -carbide due to the segregation of V [156], and the precipitated V-carbides could induce the subsequent precipitation of  $\kappa'$ -carbides in the form of band distribution [156].

Adding individual Nb/Ti, and adding compound Nb and Ti in lightweight steels can both refine grains through the precipitation of carbides, and thus enhance the yield strength of materials [1–3]. Wang et al. studied the effect of Ti addition on the mechanical properties and microstructures of Fe-30Mn-10Al-1.57C-2.3Cr-0.3Si-xTi ( $x = 0, 0.3, 0.6,$  and  $0.9$  wt%), and it was revealed that grain refinement effect become extremely obvious with increasing Ti content [100]. However, there is continuing debate as to the effect of trace element addition on the precipitation of  $\kappa'$ -carbides [142]. Li et al. found  $\kappa'$ -carbides densely distributed at the (Ti,Mo,Nb)C/ $\gamma$  interface, which could act as the nucleation site of the  $\kappa'$ -carbide [143], whereas Park et al. reported Nb addition caused the consumption of C solute atoms to form the primary and secondary NbC carbides, thus lowering the precipitation rates of  $\kappa'$ -carbide [144].

Recently, Cu addition was proposed as a promising method to achieve the high yield strengths of medium-Mn and high-Mn lightweight steels by the co-precipitation of nano-scale Cu-rich and  $\kappa'/\kappa$ -carbide particles [53,165]. Cu, as an austenite stabilizer, not only increases the volume fraction of austenite but also hinders the recrystallization due to the solute drag effect, and it promotes the formation of Cu-rich B2 particles and Cu-segregated interfacial layers [53]. Since the Cu-rich particles promoted the precipitation of nanosized  $\kappa'$ -carbide particles, the yield strength of particle-strengthened Fe-28Mn-9Al-0.8C-5Cu austenitic lightweight steel reaches 808 MPa with total elongation of more than 20% [165].

Sang-Heon Kim, Hansoo Kim, and Nack-J Kim reported a Ni-doped austenitic lightweight steel (Fe-16Mn-10Al-0.86C-5Ni) which possesses ultrahigh specific strength, good ductility and phenomenally high strain hardening owing to the unique duplex microstructure consisting of  $\gamma$ -matrix and evenly dispersed fine B2-intermetallic second phase [131]. The addition of Ni into the Fe-15Mn-10Al-0.8C lightweight steel led to the ordering of  $\alpha$ -ferrite and its transformation to stronger B2 compounds and prevented the formation of lamellar structure of  $\alpha + \kappa$  [166], and the interplay between B2 and  $\kappa$ -carbide precipitation was utilized to control the morphology and distribution of these precipitates. The initial formation of intra-/inter-granular  $\kappa'/\kappa$ -carbide particles within the hot-rolled Fe-21Mn-10Al-1C-5Ni steel is expected to increase the chemical driving force and correspondingly reduce the critical energy barrier for B2 nucleation, consequently facilitating the formation of a large fraction of B2 nanoparticles with size of 20–500 nm within austenite grains [149]. The investigation on the Fe-30Mn-10Al-0.9C-0.5Si-1.5Mo-1.5/3Ni steels demonstrates the reverse partitioning of Al from  $\kappa'$ -carbide to the  $\gamma$ -matrix through Ni addition, indicating that the affinity of Ni-Al is higher than that of C-Al [148].

## 7. Fabrication of Fe-Mn-Al-C Lightweight Steels

### 7.1. Fabrication Methods

Adding Al to steels could effectively reduce their mass density [75,167]. However, the excessive Al content can produce massive  $\text{Al}_2\text{O}_3$  and AlN inclusions which cause severe nozzle clogging and surface cracks in the continuous casting of slabs, which are great challenges for industrial production of lightweight steels [168–171]. Recently, a near-net shape approach to fabricate the lightweight steels by a near-rapid solidification process was proposed, which was conducted by the centrifugal casting (Figure 7) [50,70,84,143,165,172,173]. It was reported that such route could reduce the energy consumption during the rolling deformation and promote the near-rapidly solidified material possessed features of ultra-fine microstructure, low segregation, high solid solution, and possibly non-equilibrium or metastable phases [50,174]. It was revealed that near-rapidly solidified lightweight steels showed satisfactory mechanical properties.

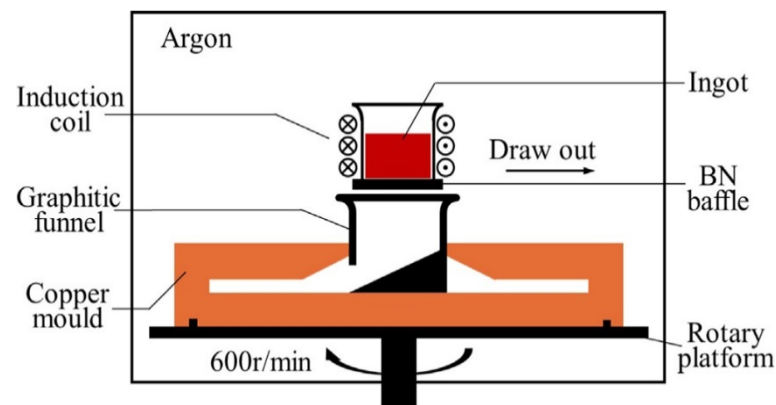


**Figure 7.** Schematic of centrifugal casting used for near-rapid solidification [84]. (Reprinted with permission from [84]. Copyright 2019 Elsevier).

### 7.2. Hot Deformation Behavior

As the TMP is a devoted part of steel production, hot deformation behaviors of high-Mn and medium-Mn Fe-Mn-Al-C lightweight steels have been investigated by several researchers [39,175–183]. The hot deformation and dynamic recrystallization (DRX) behavior of Fe-27Mn-11.5Al-0.95C steel was investigated by compressive testing in the temperature range of 900–1150 °C and strain rate of 0.01–10 s<sup>-1</sup>. Typical DRX behavior was observed and a DRX kinetics model of the steel was established [175].

The high temperature behavior of the duplex low-density Fe-18Mn-8Al-0.8C steel was investigated in the temperature range of 600–1000 °C, and a 3D processing map was developed considering the effect of strain [176]. The dynamic transformation from austenite to ferrite was found to occur in the safe efficiency domain. Therefore, the microstructure factor must be considered in the high-Mn, high-Al alloys with relatively lower Mn concentrations. Continuous dynamic recrystallization of Fe-17.5Mn-8.3Al-0.74C-0.14Si steel with a duplex microstructure was investigated [177]. The formation of progressive sub-boundaries and its effect on the materials' ductility were explored.

The hot deformation behaviors of the Fe-26Mn-8/10Al-1C steels were investigated by the 3D processing map at temperatures of 850–1050 °C and strain rates of 0.001–10 s<sup>-1</sup> and the effect of Al was considered [178]. The constitutive equations of the steels were established. The steel alloyed with more Al (i.e., 10Al steel) has a higher flow stress and a higher Z value (i.e., Zener–Hollomon parameter), indicating the increasing Al content suppressing the nucleation and growth of DRX. The number of unstable zone extends from one to two with increasing Al content and the instability region at each strain rate also increased.

As the increasing amount of C and Al together with the decreasing Mn content could facilitate the precipitation of both intra-/inter-granular  $\kappa'$ / $\kappa$ -carbides, the medium-Mn lightweight steels usually undergo hot working in the ferrite + austenite +  $\kappa$  phase region, thus resulting in complicated flow behaviors [39,43,44,180–183]. The study on the hot deformation behavior of Fe-11Mn-10Al-0.9C steel reveals the occurrence of dynamic precipitation of intra-/inter-granular  $\kappa'$ / $\kappa$ -carbides as well as discontinuous/continuous dynamic recrystallization (DDRX/CDRX) of austenite and ferrite, and a significant softening is observed, as shown in Figure 8 [181]. As the formation of inter-granular  $\kappa$ -carbide particles is detrimental to the hot workability of the medium-Mn lightweight steels [39,182], processing maps were developed by employing dynamic materials model (DMM) to determine the optimal hot deformation condition of the Fe-11Mn-10Al-0.9C steel [182]. According to the processing map, the best process window of the Fe-11Mn-10Al-0.9C steel at large strains (0.7) was identified as deformation temperature of 950–1100 °C and strain rate of 0.01–1.0 s<sup>-1</sup>; see Figure 9a. In this domain, the original coarse grains were refined, indicating that the high efficiency was dissipated by DRX (Figure 9b). Meanwhile, two unstable regions re-

sulted from inter-granular  $\kappa$ -carbides (Figure 9c) and necklace structure (Figure 9d) should be avoided during hot working.

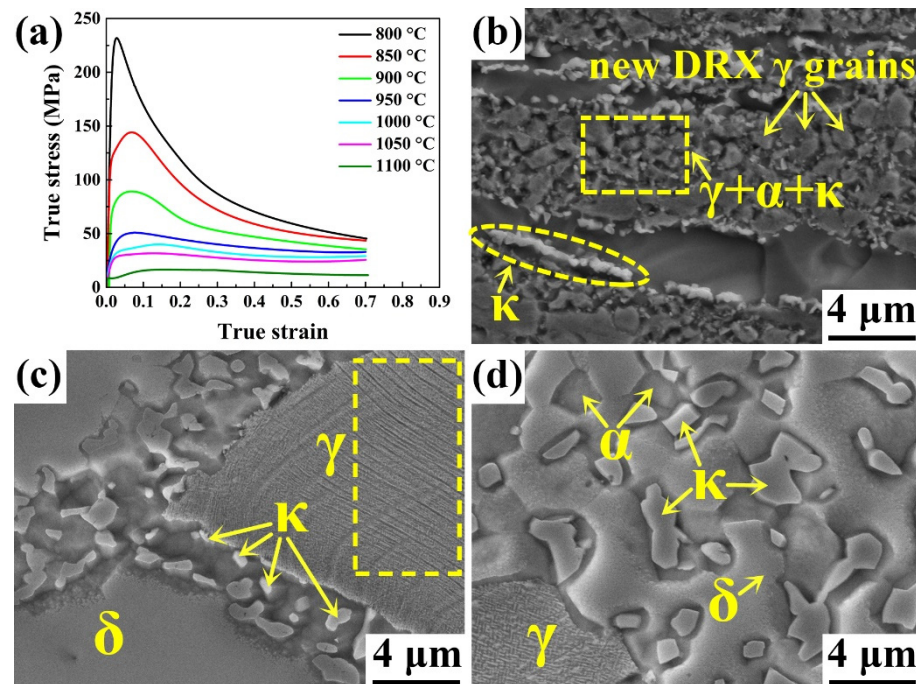


**Figure 8.** (a) Flow curves of the Fe-11Mn-10Al-0.9C medium-Mn duplex lightweight steel deformed at the strain rate of  $0.001 \text{ s}^{-1}$  and (b–d) microstructural evolution showing the dynamic precipitation of GB  $\kappa$ -carbides at the deformation temperature of  $800 \text{ }^\circ\text{C}$  under various strain rates of (b)  $10 \text{ s}^{-1}$ , (c)  $0.01 \text{ s}^{-1}$ , (d)  $0.001 \text{ s}^{-1}$  [181]. (Reproduced with permission from [181]. Copyright 2020 Elsevier).

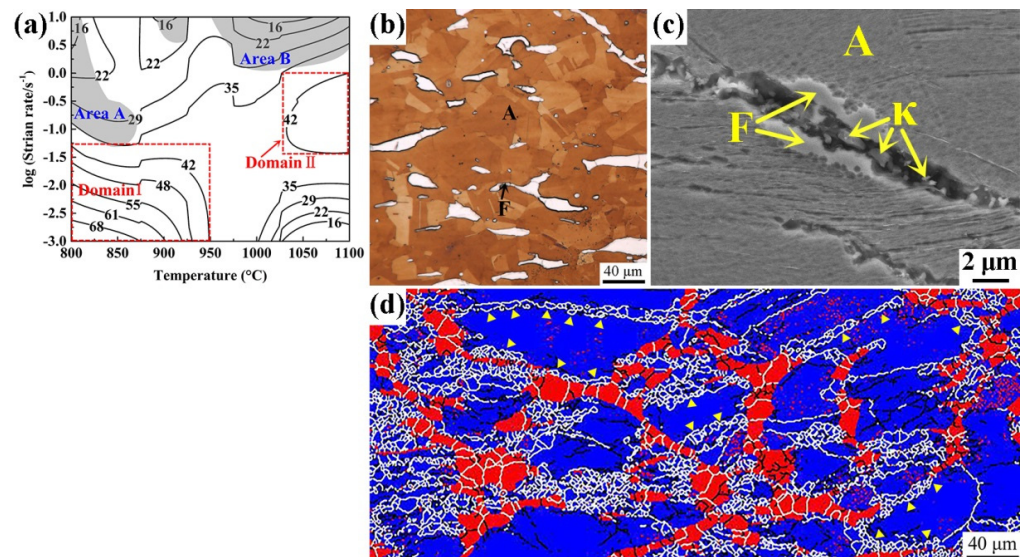


**Figure 9.** (a) The processing map the Fe-11Mn-10Al-0.9C medium-Mn duplex lightweight steel at true strain of 0.7, (b) optical image of the specimen deformed at  $1100 \text{ }^\circ\text{C}$  and  $0.1 \text{ s}^{-1}$  corresponding to Domain II showing a fine and uniform DRX microstructure, (c) scanning electron micrograph of the specimen deformed at  $800 \text{ }^\circ\text{C}$  and  $0.001 \text{ s}^{-1}$  corresponding to the instable area A showing the micro-crack induced by  $\kappa$ -carbide, and (d) the EBSD phase map of the specimen deformed at  $1000 \text{ }^\circ\text{C}$  and  $1 \text{ s}^{-1}$  corresponding to the instable area B showing the necklace structure (A: austenite, F: ferrite,  $\kappa$ :  $\kappa$ -carbide) [182]. (Reproduced with permission from [182]. Copyright 2019 Springer Nature.).

## 8. Future Research Aspects

### 8.1. Alloy Design

The variations of concentrations in Mn, Al, and C alter the phase constituents in lightweight Fe-Mn-Al-C steels and a wide range of tensile properties could be achieved. Although Al acts as an alloying element both for weight saving and microstructure modification, the limitation of additions of Al should be explored to utilize its lightweight function. The major alloying elements, Mn, Al, and C, need to be utilized properly to enhance the properties of the steels. The role of microalloying elements, such as Nb, V and Ti, in the lightweight Fe-Mn-Al-C steels should be further understood and the research of other alloying elements such as Cu, Ni, and Cr are also needed to be involved so as to optimize the overall properties and thus expand the application fields of the lightweight alloys.

### 8.2. Microstructure Design

As different phases possess different features, the coordination is needed during deformation. The stress/strain partitioning among different phases should be investigated and simulation methods might be helpful to assist the microstructure design by investigating the deformation behavior of the steels. The assessment of contributions of different strengthening mechanisms needs to be investigated for different lightweight Fe-Mn-Al-C steels.

Meanwhile, the hardening mechanisms such as the precipitation of  $\kappa$  or B2 ( $\text{DO}_3$ ) should be considered and the conditions to control of the formation of these precipitates still need to be investigated. Measures to effectively utilize these ordered intermetallics as the second phase should be explored further.

### 8.3. Comprehensive Properties

The research work on the comprehensive properties of lightweight Fe-Mn-Al-C steels is still limited. For the applications of the steels in automobile industry, investigations on the impact toughness of the materials are necessary and the formability of the materials such as hole expansion ratio and bending properties need to be evaluated and the research on high strain rate deformation is also necessary. Systematic research on the weldability and coatability of Fe-Mn-Al-C lightweight steels is also needed. To extend the applications of the steels, service properties such as fatigue, hydrogen cracking resistance, and oxidation resistance should be further investigated.

### 8.4. Fabrication Method Development

With high Mn and Al concentrations, fabrication processes such as steel making, casting, and hot rolling are facing challenges. The difficulties in fabricating the materials should be overcome in the industrial production lines. Meanwhile, new fabrication methods need to be explored. For example, 3D printing could be a promising technology for producing the newly designed Fe-Mn-Al-C steels.

## 9. Summary

- (1) In austenitic Fe-Mn-Al-C steels, the microstructure in solution treated condition is a single  $\gamma$  phase or the one with nano-sized  $\kappa'$ -carbide, depending on the compositions and heat treatment schedules. Solid solution hardening, grain size refinement, and precipitation hardening are the basic strengthening mechanisms. Measures to effectively utilize nano-sized precipitates should be explored to increase the strengths and strain hardening rates of the steels.
- (2) Austenite-based duplex Fe-Mn-Al-C steels generally possess high strength with moderate ductility. The strain partitioning between the dual phases should be investigated to guarantee the accommodation of deformation in two phases with different properties so as to achieve higher performance.

- (3) Mn and Al, the major alloying elements of the present alloy, play the opposite role on the phase stabilization of alloys as the austenite stabilizer and ferrite stabilizer, respectively. It is essential to examine the phase constituents of the steels treated with different schedules and their effects on the mechanical properties. The effects of trace elements on the mechanical properties still need to be investigated to modify the microstructures and tailor properties of the materials.
- (4) Mechanical behaviors of the Fe-Mn-Al-C steels at different temperatures and strain rates need to be investigated to meet the requirements for actual applications. Other properties such as fatigue, formability, weldability, and coatability need to be evaluated further to fulfill the requirements in the different practical uses.
- (5) The fabrications of the lightweight Fe-Mn-Al-C steels need to be explored in the conventional production line. New methods to fabricate the Fe-Mn-Al-C steels with relatively high Al concentrations need to be developed.

**Author Contributions:** Conceptualization, H.D.; methodology, H.D. and D.L.; software, H.D.; validation, H.D.; formal analysis, H.D.; investigation, H.D. and D.L.; resources, H.D.; data curation, H.D.; writing—original draft preparation, H.D. and D.L.; writing—review and editing, H.D., D.L. M.C. and Y.Z.; visualization, H.D.; supervision, H.D.; project administration, H.D.; funding acquisition, H.D. All authors have read and agreed to the published version of the manuscript.

**Funding:** This work was financially supported by grants through the National Natural Science Foundation of China (U1760205).

**Institutional Review Board Statement:** Not applicable.

**Informed Consent Statement:** Not applicable.

**Data Availability Statement:** Data sharing is not applicable to this article.

**Conflicts of Interest:** The authors declare no conflict of interest.

## References

1. Chen, S.P.; Rana, R.; Haldar, A.; Ray, R.K. Current state of Fe-Mn-Al-C low density steels. *Prog. Mater. Sci.* **2017**, *89*, 345–391. [[CrossRef](#)]
2. Ho, N.J.; Wu, L.T.; Tjong, S.C. Cyclic deformation of duplex Fe-30Mn-10Al-0.4C alloy at room temperature. *Mater. Sci. Eng.* **1988**, *102*, 49–55. [[CrossRef](#)]
3. He, L.; Jian-ping, Z.; Zhan-yu, W.; Li, D. Effect of heat treatment on cyclic deformation properties of Fe-26Mn-10Al-C steel. *J. Iron Steel Res. Int.* **2019**, *26*, 200–210.
4. Kalashnikov, I.S.; Acselrad, O.; Pereira, L.C.; Kalichak, T.; Khadyev, M.S. Behavior of Fe-Mn-Al-C steels during cyclic tests. *J. Mater. Eng. Perform.* **2000**, *9*, 334–337. [[CrossRef](#)]
5. Ho, N.J.; Tjong, S.C. Cyclic stress-strain behaviour of austenitic Fe-29.7Mn-8.7Al-1.04C alloy at room temperature. *Mater. Sci. Eng.* **1987**, *94*, 195–202. [[CrossRef](#)]
6. Chang, S.C.; Hsuis, Y.H.; Jahn, M.T. Tensile and fatigue properties of Fe-Mn-Al-C alloys. *J. Mater. Sci.* **1989**, *24*, 1117–1120. [[CrossRef](#)]
7. Sie, C.T. Dislocation microstructures in fatigued Fe-30Mn-10Al-0.4C alloy. *Phys. Status Solidi* **1990**, *121*, 119–127.
8. Yang, W.S.; Wan, C.M. High temperature studies of Fe-Mn-Al-C alloys with different manganese concentrations in air and nitrogen. *J. Mater. Sci.* **1989**, *24*, 3497–3503. [[CrossRef](#)]
9. Peng, W.; Wang, J.J.; Zhang, H.W.; Hong, X.Y.; Wu, Z.Y.; Xu, Y.L.; Li, J.; Xiao, X.S. Insights into the role of grain refinement on high-temperature initial oxidation phase transformation and oxides evolution in high aluminium Fe-Mn-Al-C duplex lightweight steel. *Corros. Sci.* **2017**, *126*, 3497–3503. [[CrossRef](#)]
10. Huang, Z.Y.; Jiang, Y.S.; Hou, A.L.; Wang, P.; Shi, Q.; Hou, Q.Y.; Liu, X.H. Rietveld refinement, microstructure and high-temperature oxidation characteristics of low-density high manganese steels. *J. Mater. Sci. Technol.* **2017**, *33*, 1531–1539. [[CrossRef](#)]
11. Wang, C.J.; Chang, Y.C. Formation and growth morphology of nodules in the high-temperature oxidation of Fe-Mn-Al-C alloy. *Mater. Chem. Phys.* **2003**, *77*, 738–743. [[CrossRef](#)]
12. Balaško, T.; Šetina, B.B.; Medved, J.; Burja, J. High-Temperature Oxidation Behaviour of Duplex Fe-Mn-Al-Ni-C Lightweight Steel. *Crystals* **2022**, *12*, 957. [[CrossRef](#)]
13. Rana, R.; Liu, C.; Ray, R.K. Low-density low-carbon Fe-Al ferritic steels. *Scr. Mater.* **2013**, *68*, 354–359. [[CrossRef](#)]
14. Janda, D.; Ghassemi-Armaki, H.; Bruder, E.; Hockauf, M.; Heilmaier, M.; Kumar, K.S. Effect of strain-rate on the deformation response of D0<sub>3</sub>-ordered Fe<sub>3</sub>Al. *Acta Mater.* **2016**, *103*, 909–918. [[CrossRef](#)]

15. Herrmann, J.; Inden, G.; Sauthoff, G. Deformation behaviour of iron-rich iron-aluminum alloys at low temperatures. *Acta Mater.* **2003**, *51*, 2847–2857. [[CrossRef](#)]
16. Zargaran, A.; Kim, H.S.; Kwak, J.H.; Kim, N.J. Effects of Nb and C additions on the microstructure and tensile properties of lightweight ferritic Fe-8Al-5Mn alloy. *Scr. Mater.* **2014**, *89*, 37–40. [[CrossRef](#)]
17. Castan, C.; Montheillet, F.; Perlade, A. Dynamic recrystallization mechanisms of an Fe-8% Al low density steel under hot rolling conditions. *Scr. Mater.* **2013**, *68*, 360–364. [[CrossRef](#)]
18. Min, C.H.; Koo, J.-M.; Lee, J.-K.; Si, W.H.; Park, K.-T. Tensile deformation of a low density Fe-27Mn-12Al-0.8C duplex steel in association with ordered phases at ambient temperature. *Mater. Sci. Eng.* **2013**, *586*, 276–283.
19. Łyszkowski, R.; Bystrzycki, J. Hot deformation and processing maps of a Fe-Al intermetallic alloy. *Mater. Charact.* **2014**, *96*, 196–205. [[CrossRef](#)]
20. Łyszkowski, R.; Czujko, T.; Varin, R.A. Multi-axial forging of Fe<sub>3</sub>Al-base intermetallic alloy and its mechanical properties. *J. Mater. Sci.* **2017**, *52*, 2902–2914. [[CrossRef](#)]
21. Rana, R.; Liu, C.; Ray, R.K. Evolution of microstructure and mechanical properties during thermomechanical processing of a low-density multiphase steel for automotive application. *Acta Mater.* **2014**, *75*, 227–245. [[CrossRef](#)]
22. Seol, J.-B.; Raabe, D.; Choi, P.; Park, H.-S.; Kwak, J.-H.; Park, C.-G. Direct evidence for the formation of ordered carbides in a ferrite-based low-density Fe-Mn-Al-C alloy studied by transmission electron microscopy and atom probe tomography. *Scr. Mater.* **2013**, *68*, 348–353. [[CrossRef](#)]
23. Han, S.Y.; Shin, S.Y.; Lee, S.; Kim, N.J.; Kwak, J.-H.; Chin, K.-G. Effect of Carbon Content on Cracking Phenomenon Occurring during Cold Rolling of Three Light-Weight Steel Plates. *Metall. Mater. Trans.* **2011**, *42*, 138–146. [[CrossRef](#)]
24. Sohn, S.S.; Lee, B.-J.; Lee, S.; Kwak, J.-H. Effect of Mn Addition on Microstructural Modification and Cracking Behavior of Ferritic Light-Weight Steels. *Metall. Mater. Trans.* **2014**, *45*, 5469–5485. [[CrossRef](#)]
25. Sohn, S.S.; Lee, B.-J.; Lee, S.; Kwak, J.-H. Effects of aluminum content on cracking phenomenon occurring during cold rolling of three ferrite-based lightweight steel. *Acta Mater.* **2013**, *61*, 5626–5635. [[CrossRef](#)]
26. Shin, S.Y.; Lee, H.; Han, S.Y.; Seo, C.-H.; Choi, K.; Lee, S.; Kim, N.J.; Kwak, J.-H.; Chin, K.-G. Correlation of Microstructure and Cracking Phenomenon Occurring during Hot Rolling of Lightweight Steel Plates. *Metall. Mater. Trans.* **2010**, *41*, 138. [[CrossRef](#)]
27. Sohn, S.S.; Lee, B.-H.; Lee, S.; Kim, N.J.; Kwak, J.-H. Effect of annealing temperature on microstructural modification and tensile properties in 0.35C-3.5Mn-5.8Al lightweight steel. *Acta Mater.* **2013**, *61*, 5050–5066. [[CrossRef](#)]
28. Seo, C.-H.; Kwon, K.H.; Choi, K.; Kim, K.-H.; Kwak, J.-H.; Lee, S.; Kim, N.J. Deformation behavior of ferrite-austenite duplex lightweight Fe-Mn-Al-C steel. *Scr. Mater.* **2012**, *66*, 519–522. [[CrossRef](#)]
29. Sohn, S.S.; Choi, K.; Kwak, J.-H.; Kim, N.J.; Lee, S. Novel ferrite-austenite duplex lightweight steel with 77% ductility by transformation induced plasticity and twinning induced plasticity mechanisms. *Acta Mater.* **2014**, *78*, 181–189. [[CrossRef](#)]
30. Park, S.J.; Hwang, B.; Lee, K.H.; Lee, T.H.; Suh, D.W.; Han, H.N. Microstructure and tensile behavior of duplex low-density steel containing 5mass% aluminum. *Scr. Mater.* **2013**, *68*, 365–369. [[CrossRef](#)]
31. Jeong, J.; Lee, C.-Y.; Park, I.-J.; Lee, Y.-K. Isothermal precipitation behavior of  $\kappa$ -carbide in the Fe-9Mn-6Al-0.15C lightweight steel with a multiphase microstructure. *J. Alloy Compd.* **2013**, *574*, 299–304. [[CrossRef](#)]
32. Lee, S.; Jeong, J.; Lee, Y.-K. Precipitation and dissolution behavior of  $\kappa$ -carbide during continuous heating in Fe-9.3Mn-5.6Al-0.16C lightweight steel. *J. Alloy Compd.* **2015**, *648*, 149–153. [[CrossRef](#)]
33. Rigaud, V.; Daloz, D.; Drillet, J.; Perlade, A.; Maugis, P.; Lesoult, G. Phases Equilibrium Study in Quaternary Iron-rich Fe-Al-Mn-C Alloys. *ISIJ Int.* **2007**, *47*, 898–906. [[CrossRef](#)]
34. Sohn, S.S.; Song, H.; Kim, J.G.; Kwak, J.-H.; Kim, H.S.; Lee, S. Effects of Annealing Treatment Prior to Cold Rolling on Delayed Fracture Properties in Ferrite-Austenite Duplex Lightweight Steels. *Metall. Mater. Trans.* **2016**, *47*, 706–717. [[CrossRef](#)]
35. Han, S.Y.; Shin, S.Y.; Lee, H.-J.; Lee, B.-J.; Lee, S.; Kim, N.J.; Kwak, J.-H. Effects of Annealing Temperature on Microstructure and Tensile Properties in Ferritic Lightweight Steels. *Metall. Mater. Trans.* **2012**, *43*, 843–853. [[CrossRef](#)]
36. Li, X.; Song, R.B.; Zhou, N.P.; Li, J.J. Microstructure and tensile behavior of Fe-8Mn-6Al-0.2C low density steel. *Mater. Sci. Eng.* **2018**, *709*, 97–104. [[CrossRef](#)]
37. Jung, H.; Lee, G.; Koo, M.; Song, H.; Ko, W.S.; Sohn, S.S. Effects of Mn Segregations on Intergranular Fracture in a Medium-Mn Low-Density Steel. *Steel Res. Int.* **2022**, 2200240. [[CrossRef](#)]
38. Zhou, N.P.; Song, R.B.; Li, X.; Li, J.J. Dependence of austenite stability and deformation behavior on tempering time in an ultrahigh strength medium Mn TRIP steel. *Mater. Sci. Eng.* **2018**, *738*, 153–162. [[CrossRef](#)]
39. Mozumder, Y.H.; Babu, K.A.; Saha, R.; Mandal, S. Flow characteristics and hot workability studies of a Ni-containing Fe-Mn-Al-C lightweight duplex steel. *Mater. Charact.* **2018**, *146*, 1–14. [[CrossRef](#)]
40. Zhao, C.; Song, R.B.; Zhang, L.F.; Yang, F.Q.; Kang, T. Effect of annealing temperature on the microstructure and tensile properties of Fe-10Mn-10Al-0.7C low-density steel. *Mater. Des.* **2016**, *91*, 348–360. [[CrossRef](#)]
41. Liu, D.G.; Cai, M.H.; Ding, H.; Han, D. Control of inter/intra-granular  $\kappa$ -carbides and its influence on overall mechanical properties of a Fe-11Mn-10Al-1.25C low density steel. *Mater. Sci. Eng.* **2018**, *715*, 25–32. [[CrossRef](#)]
42. Liu, D.G.; Ding, H.; Cai, M.H.; Han, D. Mechanical behaviors of a lower-Mn-added Fe-11Mn-10Al-1.25C lightweight steel with distinguished microstructural features. *Mater. Lett.* **2019**, *242*, 131–134. [[CrossRef](#)]

43. Lee, Y.; Kim, J.N.; Kim, G.; Lee, T.; Lee, C.S. Improved cold-rollability of duplex lightweight steels utilizing deformation-induced ferritic transformation. *Mater. Sci. Eng.* **2019**, *742*, 835–841.
44. Lee, C.-Y.; Lee, Y.-K. The Solidification Mode of Fe-Mn-Al-C Lightweight Steel. *JOM* **2014**, *66*, 1821–1827. [[CrossRef](#)]
45. Liu, D.G.; Ding, H.; Han, D.; Cai, M.H.; Lee, Y.K. Microstructural evolution and tensile properties of Fe-11Mn-10Al-1.2C medium-Mn lightweight steel. *Mater. Sci. Eng.* **2020**, *797*, 140256. [[CrossRef](#)]
46. Liu, D.G.; Ding, H.; Han, D.; Cai, M.H. Improvement of the yield strength of Fe-11Mn-xAl-yC medium-Mn lightweight steels by tuning partial recrystallization and intra-granular  $\kappa$ -carbide strengthening. *Mater. Sci. Eng.* **2022**, *833*, 142553. [[CrossRef](#)]
47. Sohn, S.S.; Song, H.; Jo, M.C.; Song, T.; Kim, H.S.; Lee, S. Novel 1.5 GPa-strength with 50%-ductility by transformation-induced plasticity of non-recrystallized austenite in duplex steels. *Sci. Rep.* **2017**, *7*, 1255. [[CrossRef](#)]
48. Sohn, S.S.; Song, H.; Kwak, J.-H.; Lee, S. Dramatic improvement of strain hardening and ductility to 95% in highly-deformable high-strength duplex lightweight steels. *Sci. Rep.* **2017**, *7*, 1927. [[CrossRef](#)]
49. Liu, M.X.; Zhou, J.Y.; Zhang, J.K.; Song, C.J.; Zhai, Q.J. Ultra-high strength medium-Mn lightweight steel by dislocation slip band refinement and suppressed intergranular  $\kappa$ -carbide with Cr addition. *Mater. Charact.* **2022**, *190*, 112042. [[CrossRef](#)]
50. He, W.; Wang, B.L.; Yang, Y.; Zhang, Y.H.; Duan, L.; Luo, Z.P.; Song, C.J.; Zhai, Q.J. Microstructure and mechanical behavior of a low-density Fe-12Mn-9Al-1.2C steel prepared using centrifugal casting under near-rapid solidification. *J. Iron Steel Res. Int.* **2018**, *25*, 830–838.
51. Sohn, S.S.; Song, H.; Suh, B.C.; Kwak, J.H.; Lee, B.J.; Kim, N.J.; Lee, S. Novel ultra-high-strength (ferrite plus austenite) duplex lightweight steels achieved by fine dislocation substructures (Taylor lattices), grain refinement, and partial recrystallization. *Acta Mater.* **2015**, *96*, 301–310. [[CrossRef](#)]
52. Liu, S.; Ge, Y.L.; Liu, H.Y.; Liu, J.Y.; Feng, Y.L.; Chen, C.; Zhang, F.C. Tensile Properties and Microstructure Evolutions of Low-Density Duplex Fe-12Mn-7Al-0.2C-0.6Si Steel. *Materials* **2022**, *15*, 2498. [[CrossRef](#)]
53. Song, H.J.; Yoo, J.; Kim, S.H.; Sohn, S.S.; Koo, M.; Kim, N.J.; Lee, S. Novel ultra-high-strength Cu-containing medium-Mn duplex lightweight steels. *Acta Mater.* **2017**, *135*, 215–225. [[CrossRef](#)]
54. Wu, Z.Q.; Ding, H.; Li, H.Y.; Huang, M.L.; Cao, F.R. Microstructural evolution and strain hardening behavior during plastic deformation of Fe-12Mn-8Al-0.8C steel. *Mater. Sci. Eng.* **2013**, *584*, 150–155. [[CrossRef](#)]
55. Song, H.; Kwon, Y.; Sohn, S.S.; Koo, M.; Kim, N.J.; Lee, B.J.; Lee, S. Improvement of tensile properties in (austenite + ferrite +  $\kappa$ -carbide) triplex hot-rolled lightweight steels. *Mater. Sci. Eng.* **2018**, *730*, 177–186.
56. Song, H.; Jo, M.; Kim, D.W. Vanadium or copper alloyed duplex lightweight steel with enhanced hydrogen embrittlement resistance at room temperature. *Mater. Sci. Eng.* **2021**, *817*, 141347. [[CrossRef](#)]
57. Han, D.; Ding, H.; Liu, D.G.; Rolfe, B.; Beladi, H. Influence of C content and annealing temperature on the microstructures and tensile properties of Fe-13Mn-8Al-(0.7,1.2)C steels. *Mater. Sci. Eng.* **2020**, *785*, 139286. [[CrossRef](#)]
58. Han, D.; Ding, H.; Liu, D.G. The microstructures and tensile properties of aged Fe-xMn-8Al-0.8C low-density steels. *Mater. Sci. Technol.* **2020**, *36*, 681–689. [[CrossRef](#)]
59. Chen, W.C.; Wu, C.C.; Chang, W.Y. Effects of Aging Treatment on Microstructure of High-Al-content Fe-15Mn-10Al-1.0C Alloy. *Sens. Mater.* **2018**, *30*, 515–523.
60. Yang, M.X.; Yuan, F.P.; Xie, Q.G.; Wang, Y.D.; Ma, E.; Wu, X.L. Strain hardening in Fe-16Mn-10Al-0.86C-5Ni high specific strength steel. *Acta Mater.* **2016**, *109*, 213–222. [[CrossRef](#)]
61. Kumar, N.; Singh, K.; Singh, A. Microstructural evolution after heat treatment of high specific strength steel: Fe-13Al-16Mn-5Ni-0.8C and correlation with tensile properties. *Materialia* **2022**, *22*, 101412. [[CrossRef](#)]
62. Cheng, W.-C. Phase Transformations of an Fe-0.85C-17.9Mn-7.1Al Austenitic Steel After Quenching and Annealing. *JOM* **2014**, *66*, 1809–1820. [[CrossRef](#)]
63. Ding, H.; Han, D.; Zhang, J.; Cai, Z.H.; Wu, Z.Q.; Cai, M.H. Tensile deformation behavior analysis of low density Fe-18Mn-10Al-xC steels. *Mater. Sci. Eng.* **2016**, *652*, 69–76. [[CrossRef](#)]
64. Ding, H.; Han, D.; Cai, Z.H.; Wu, Z.Q. Microstructures and Mechanical Behavior of Fe-18Mn-10Al-(0.8-1.2)C Steels. *JOM* **2014**, *66*, 1821–1827. [[CrossRef](#)]
65. Huo, Y.T.; He, Y.L.; Zhu, N.Q.; Ding, M.L.; Liu, R.D.; Zhang, Y. Deformation Mechanism Investigation on Low Density 18Mn Steels under Different Solid Solution Treatments. *Metals* **2021**, *11*, 1497. [[CrossRef](#)]
66. Piston, M.; Bartlett, L.; Limmer, K.R.; Field, D.M. Microstructural Influence on Mechanical Properties of a Lightweight Ultrahigh Strength Fe-18Mn-10Al-0.9C-5Ni (wt%) Steel. *Metals* **2020**, *10*, 1305. [[CrossRef](#)]
67. Hwang, S.W.; Ji, J.H.; Lee, E.G.; Park, K.T. Tensile deformation of a duplex Fe-20Mn-9Al-0.6C steel having the reduced specific weight. *Mater. Sci. Eng.* **2011**, *528*, 5196–5203. [[CrossRef](#)]
68. Ma, B.; Li, C.S.; Zheng, J.J.; Song, Y.L.; Han, Y.H. Strain hardening behavior and deformation substructure of Fe-20/27Mn-4Al-0.3C non-magnetic steels. *Mater. Des.* **2016**, *92*, 313–321. [[CrossRef](#)]
69. Sutou, Y.; Kamiya, N.; Umino, R.; Ohnuma, I.; Ishida, K. High-strength Fe-20Mn-Al-C-based Alloys with Low Density. *ISIJ Int.* **2010**, *50*, 893–899. [[CrossRef](#)]
70. Liu, L.B.; Li, C.M.; Yang, Y.; Luo, Z.P.; Song, C.J.; Zhai, Q.J. A simple method to produce austenite-based low-density Fe-20Mn-9Al-0.75C steel by a near-rapid solidification process. *Mater. Sci. Eng.* **2017**, *679*, 282–291. [[CrossRef](#)]
71. Ma, B.; Li, C.S.; Song, Y.L.; Zheng, J.J. Effect of manganese content on hot deformation behaviour of Fe-(20/27)Mn-4Al-0.3C non-magnetic steels. *Mater. Sci. Technol.* **2016**, *32*, 890–897. [[CrossRef](#)]

72. Lee, S.I.; Lee, S.W.; Kim, S.G.; Hwang, B. Correlation of Delta-Ferrite with Tensile and Charpy Impact Properties of Austenitic Fe-23Mn-Al-C Steels. *Metall. Mater. Trans.* **2021**, *52*, 4170–4180. [[CrossRef](#)]
73. Feng, Y.F.; Song, R.B.; Pei, Z.Z.; Song, R.F.; Dou, G.Y. Effect of Aging Isothermal Time on the Microstructure and Room-Temperature Impact Toughness of Fe-24.8Mn-7.3Al-1.2C Austenitic Steel with kappa-Carbides Precipitation. *Met. Mater. Int.* **2018**, *24*, 1012–1023. [[CrossRef](#)]
74. Ding, H.; Li, H.Y.; Misra, R.D.K.; Wu, Z.Q.; Cai, M.H. Strengthening Mechanisms in Low Density Fe-26Mn-xAl-1C Steels. *Steel Res. Int.* **2018**, *89*, 1700381. [[CrossRef](#)]
75. Frommeyer, G.; Brux, U. Microstructures and mechanical properties of high-strength Fe-Mn-Al-C light-weight TRIPLEX steels. *Steel Res. Int.* **2006**, *77*, 627–633. [[CrossRef](#)]
76. Yang, F.Q.; Song, R.B.; Li, Y.P.; Sun, T.; Wang, K.K. Tensile deformation of low density duplex Fe-Mn-Al-C steel. *Mater. Des.* **2015**, *76*, 32–39. [[CrossRef](#)]
77. Zhang, L.F.; Song, R.B.; Zhao, C.; Yang, F.Q. Work hardening behavior involving the substructural evolution of an austenite-ferrite Fe-Mn-Al-C steel. *Mater. Sci. Eng.* **2015**, *640*, 225–234. [[CrossRef](#)]
78. Park, K.T.; Hwang, S.W.; Son, C.Y.; Lee, J.K. Effects of Heat Treatment on Microstructure and Tensile Properties of a Fe-27Mn-12Al-0.8C Low-Density Steel. *JOM* **2014**, *66*, 1828–1836. [[CrossRef](#)]
79. Etienne, A.; Massardier-Jourdan, V.; Cazottes, S.; Garat, X.; Soler, M.; Zuazo, I.; Kleber, X. Ferrite Effects in Fe-Mn-Al-C Triplex Steels. *Metall. Mater. Trans.* **2014**, *45A*, 324–334. [[CrossRef](#)]
80. Zhang, L.F.; Song, R.B.; Zhao, C.; Yang, F.Q.; Xu, Y.; Peng, S.G. Evolution of the microstructure and mechanical properties of an austenite-ferrite Fe-Mn-Al-C steel. *Mater. Sci. Eng.* **2015**, *643*, 183–193. [[CrossRef](#)]
81. Song, H.; Yoo, J.; Sohn, S.S.; Koo, M.; Lee, S. Achievement of high yield strength and strain hardening rate by forming fine ferrite and dislocation substructures in duplex lightweight steel. *Mater. Sci. Eng.* **2017**, *704*, 287–291. [[CrossRef](#)]
82. Lee, K.; Park, S.J.; Kang, J.Y.; Park, S.; Han, S.S.; Park, J.Y.; Oh, K.H.; Lee, S.; Rollett, A.D.; Han, H.N. Investigation of the aging behavior and orientation relationships in Fe-31.4Mn-11.4Al-0.89C low-density steel. *J. Alloy Compd.* **2017**, *723*, 146–156. [[CrossRef](#)]
83. Xie, Z.Q.; Hui, W.J.; Zhang, Y.J.; Zhao, X.L. Effect of Cu and solid solution temperature on microstructure and mechanical properties of Fe-Mn-Al-C low-density steels. *J. Mater. Res. Technol.* **2022**, *18*, 1307–1321. [[CrossRef](#)]
84. Yang, Y.; Zhang, J.; Hu, C.; Luo, Z.; Zhang, Y.; Song, C.; Zhai, Q. Structures and properties of Fe-(8–16)Mn-9Al-0.8 C low density steel made by a centrifugal casting in near-rapid solidification. *Mater. Sci. Eng.* **2019**, *748*, 74–84. [[CrossRef](#)]
85. Kim, C.; Terner, M.; Hong, H.-U.; Lee, C.-H.; Park, S.-J.; Moon, J. Influence of inter/intra-granular  $\kappa$ -carbides on the deformation mechanism in lightweight Fe-20Mn-11.5Al-1.2C steel. *Mater. Charact.* **2020**, *161*, 110142. [[CrossRef](#)]
86. Park, K.-T.; Jin, K.G.; Han, S.H.; Hwang, S.W.; Choi, K.; Lee, C.S. Stacking fault energy and plastic deformation of fully austenitic high manganese steels: Effect of Al addition. *Mater. Sci. Eng.* **2010**, *527*, 3651–3661. [[CrossRef](#)]
87. Yoo, J.D.; Park, K.T. Microband-induced plasticity in a high Mn-Al-C light steel. *Mater. Sci. Eng.* **2008**, *496*, 417–424. [[CrossRef](#)]
88. Yoo, J.D.; Hwang, S.W.; Park, K.T. Origin of Extended Tensile Ductility of a Fe-28Mn-10Al-1C Steel. *Metall. Mater. Trans.* **2009**, *40A*, 1520–1523. [[CrossRef](#)]
89. Park, K.T. Tensile deformation of low-density Fe-Mn-Al-C austenitic steels at ambient temperature. *Scr. Mater.* **2013**, *68*, 375–379. [[CrossRef](#)]
90. Choi, K.; See, C.H.; Lee, H.; Kim, S.K.; Kwak, J.H.; Chin, K.G.; Park, K.T.; Kim, N.J. Effect of aging on the microstructure and deformation behavior of austenite base lightweight Fe-28Mn-9Al-0.8C steel. *Scr. Mater.* **2010**, *63*, 1028–1031. [[CrossRef](#)]
91. Chang, K.M.; Chao, C.G.; Liu, T.F. Excellent combination of strength and ductility in an Fe-9Al-28Mn-1.8C alloy. *Scr. Mater.* **2010**, *63*, 162–165. [[CrossRef](#)]
92. Lin, C.L.; Chao, C.G.; Bor, H.Y.; Liu, T.F. Relationship between Microstructures and Tensile Properties of an Fe-30Mn-8.5Al-2.0C Alloy. *Mater. Trans.* **2010**, *51*, 1084–1088. [[CrossRef](#)]
93. Lin, C.L.; Chao, C.G.; Juang, J.Y.; Yang, J.M.; Liu, T.F. Deformation mechanisms in ultrahigh-strength and high-ductility nanostructured FeMnAlC alloy. *J. Alloy Compd.* **2014**, *586*, 616–620. [[CrossRef](#)]
94. Gutierrez-Urrutia, I.; Raabe, D. Multistage strain hardening through dislocation substructure and twinning in a high strength and ductile weight-reduced Fe-Mn-Al-C steel. *Acta Mater.* **2012**, *60*, 5791–5802. [[CrossRef](#)]
95. Gutierrez-Urrutia, I.; Raabe, D. High strength and ductile low density austenitic FeMnAlC steels: Simplex and alloys strengthened by nanoscale ordered carbides. *Mater. Sci. Technol.* **2014**, *30*, 1099–1104. [[CrossRef](#)]
96. Springer, H.; Raabe, D. Compositional and thermo-mechanical high throughput bulk combinatorial design of structural materials based on the example of 30Mn-1.2C-xAl triplex steels. *Acta Mater.* **2012**, *60*, 4950–4959. [[CrossRef](#)]
97. Welsch, E.; Ponge, D.; Haghighat, S.M.H.; Sandlobes, S.; Choi, P.; Herbig, M.; Zaeferrer, S.; Raabe, D. Strain hardening by dynamic slip band refinement in a high-Mn lightweight steel. *Acta Mater.* **2016**, *116*, 188–199. [[CrossRef](#)]
98. Lai, H.J.; Wan, C.M. The study of work hardening in Fe-Mn-Al-C alloys. *J. Mater. Sci.* **1989**, *24*, 3407–3412. [[CrossRef](#)]
99. Choo, W.K.; Kim, J.H.; Yoon, J.C. Microstructural change in austenitic Fe-30.0wt%Mn-7.8wt%Al-1.3wt%C initiated by spinodal decomposition and its influence on mechanical properties. *Acta Mater.* **1997**, *45*, 4877–4885. [[CrossRef](#)]
100. Wang, F.; Wang, S.T.; Chen, B.H.; Ma, W.; Jing, Q.; Zhang, X.Y.; Ma, M.Z.; Wang, Q.F.; Liu, R.P. Effect of Ti addition on the mechanical properties and microstructure of novel Al-rich low-density multi-principal-element alloys. *J. Alloy Compd.* **2022**, *891*, 162028. [[CrossRef](#)]

101. Wan, P.; Kang, T.; Li, F.; Gao, P.F.; Zhang, L.; Zhao, Z.Z. Dynamic recrystallization behavior and microstructure evolution of low-density high-strength Fe-Mn-Al-C steel. *J. Mater. Res. Technol.* **2021**, *15*, 1059–1068. [[CrossRef](#)]
102. Wang, H.; Gao, Z.Y.; Shi, Z.Y.; Xu, H.F.; Zhang, L.; Wu, G.L.; Wang, C.; Wang, C.Y.; Weng, Y.Q.; Cao, W.Q. High Temperature Deformation Behavior and Microstructure Evolution of Low-Density Steel Fe<sub>30</sub>Mn<sub>11</sub>Al<sub>1</sub>C Micro-Alloyed with Nb and V. *Materials* **2021**, *14*, 6555. [[CrossRef](#)] [[PubMed](#)]
103. Liu, J.X.; Wu, H.B.; He, J.S.; Yang, S.W.; Ding, C. Effect of  $\kappa$ -carbides on the mechanical properties and superparamagnetism of Fe-28Mn-11Al-1.5/1.7C-5Cr lightweight steels. *Mater. Sci. Eng.* **2022**, *849*, 143462. [[CrossRef](#)]
104. Xing, J.; Hou, L.F.; Du, H.Y.; Liu, B.S.; Wei, Y.H. A New Explanation for the Effect of Dynamic Strain Aging on Negative Strain Rate Sensitivity in Fe-30Mn-9Al-1C Steel. *Materials* **2019**, *12*, 3426. [[CrossRef](#)] [[PubMed](#)]
105. Wu, H.; Tan, Y.; Malik, A.; Wang, Y.W.; Naqvi, S.Z.H.; Cheng, H.W.; Tian, J.B.; Meng, X.M. Dynamic Compressive Mechanical Behavior and Microstructure Evolution of Rolled Fe-28Mn-10Al-1.2C Low-Density Steel. *Material* **2022**, *15*, 3550. [[CrossRef](#)]
106. Feng, Y.F.; Song, R.B.; Wang, Y.J.; Liu, M.; Li, H.; Liu, X.G. Aging hardening and precipitation behavior of Fe-31.6Mn-8.8Al-1.38C austenitic cast steel. *Vacuum* **2020**, *181*, 109662. [[CrossRef](#)]
107. Wu, Z.Q.; Ding, H.; An, X.H.; Han, D.; Liao, X.Z. Influence of Al content on the strain-hardening behavior of aged low density Fe-Mn-Al-C steels with high Al content. *Mater. Sci. Eng.* **2015**, *639*, 187–191. [[CrossRef](#)]
108. Wang, F.; An, Z.L.; Wang, S.T.; Ji, P.F.; Li, B.; Jing, Q.; Zhang, X.Y.; Ma, M.Z.; Wang, Q.F.; Liu, R.P. Effect of Different Hot Deformation Temperatures on the Microstructure and Mechanical Properties of High Al/Mn Lightweight Steel. *J. Mater. Eng. Perform.* **2022**, *31*, 3799–3810. [[CrossRef](#)]
109. Ma, L.; Tang, Z.Y.; You, Z.Y.; Guan, G.F.; Ding, H.; Misra, D. Microstructure, Mechanical Properties and Deformation Behavior of Fe-28.7Mn-10.2Al-1.06C High Specific Strength Steel. *Metals* **2022**, *12*, 602. [[CrossRef](#)]
110. Ren, P.; Chen, X.P.; Mei, L.; Nie, Y.Y.; Cao, W.Q.; Liu, Q. Intragranular brittle precipitates improve strain hardening capability of Fe-30Mn-11Al-1.2C low-density steel. *Mater. Sci. Eng.* **2020**, *775*, 138984. [[CrossRef](#)]
111. Zhang, J.L.; Raabe, D.; Tasan, C.C. Designing duplex, ultrafine-grained Fe-Mn-Al-C steels by tuning phase transformation and recrystallization kinetics. *Acta Mater.* **2017**, *141*, 374–387. [[CrossRef](#)]
112. Chen, X.P.; Xu, Y.P.; Ren, P.; Li, W.J.; Cao, W.Q.; Liu, Q. Aging hardening response and  $\beta$ -Mn transformation behavior of high carbon high manganese austenitic low-density Fe-30Mn-10Al-2C steel. *Mater. Sci. Eng.* **2017**, *703*, 167–172. [[CrossRef](#)]
113. Kang, L.; Yuan, H.; Li, H.Y.; Ji, Y.F.; Liu, H.T.; Liu, G.M. Enhanced Mechanical Properties of Fe-Mn-Al-C Low Density Steel via Aging Treatment. *Front. Mater.* **2021**, *8*, 680776. [[CrossRef](#)]
114. Zhang, J.L.; Jiang, Y.S.; Zheng, W.S.; Liu, Y.X.; Addad, A.; Ji, G.; Song, C.J.; Zhai, Q.J. Revisiting the formation mechanism of intragranular  $\kappa$ -carbide in austenite of a Fe-Mn-Al-Cr-C low-density steel. *Scr. Mater.* **2021**, *199*, 113836. [[CrossRef](#)]
115. Ren, P.; Chen, X.P.; Wang, C.Y.; Zhou, Y.X.; Cao, W.Q.; Liu, Q. Evolution of microstructure, texture and mechanical properties of Fe-30Mn-11Al-1.2C low-density steel during cold rolling. *Mater. Charact.* **2021**, *174*, 111013. [[CrossRef](#)]
116. Yao, M.J.; Welsch, E.; Ponge, D.; Haghighat, S.M.H.; Sandlobes, S.; Choi, P.; Herbig, M.; Bleskov, I.; Hickel, T.; Lipinska-Chwalek, M.; et al. Strengthening and strain hardening mechanisms in a precipitation-hardened high-Mn lightweight steel. *Acta Mater.* **2017**, *140*, 258–273. [[CrossRef](#)]
117. Pang, J.Y.; Zhou, Z.M.; Zhao, Z.Z.; Tang, D.; Liang, J.H.; He, Q. Tensile Behavior and Deformation Mechanism of Fe-Mn-Al-C Low Density Steel with High Strength and High Plasticity. *Metals* **2019**, *9*, 897. [[CrossRef](#)]
118. Kim, B.; Jeong, S.; Park, S.-J.; Moon, J.; Lee, C. Roles of (Fe, Mn)<sub>3</sub>Al Precipitates and MBIP on the Hot Ductility Behavior of Fe-30Mn-9Al-0.9C Lightweight Steels. *Met. Mater. Int.* **2019**, *25*, 1019–1026. [[CrossRef](#)]
119. Wang, C.S.; Hwang, C.N.; Chao, C.G.; Liu, T.F. Phase transitions in an Fe-9Al-30Mn-2.0C alloy. *Scr. Mater.* **2007**, *57*, 809–812. [[CrossRef](#)]
120. Kim, C.W.; Ternner, M.; Lee, J.H.; Hong, H.U.; Moon, J.; Park, S.J.; Jang, J.H.; Lee, C.H.; Lee, B.H.; Lee, Y.J. Partitioning of C into  $\kappa$ -carbides by Si addition and its effect on the initial deformation mechanism of Fe-Mn-Al-C lightweight steels. *J. Alloy Compd.* **2019**, *775*, 554–564. [[CrossRef](#)]
121. Yoo, J.D.; Hwang, S.W.; Park, K.T. Factors influencing the tensile behavior of a Fe-28Mn-9Al-0.8C steel. *Mater. Sci. Eng.* **2009**, *508*, 234–240. [[CrossRef](#)]
122. Christian, H.; Christoffer, Z.; Tobias, I.; André, B.; Florian, T.; Bengt, H.; Weiping, H.; Wolfgang, B.; Dmitri, A.M. On the deformation behavior of  $\kappa$ -carbide-free and  $\kappa$ -carbide-containing high-Mn light-weight steel. *Acta Mater.* **2017**, *122*, 332–343.
123. Park, S.W.; Park, J.Y.; Cho, K.M.; Jang, J.H.; Park, S.J.; Moon, J.; Lee, T.H.; Shin, J.H. Effect of Mn and C on Age Hardening of Fe-Mn-Al-C Lightweight Steels. *Met. Mater. Int.* **2019**, *25*, 683–696. [[CrossRef](#)]
124. Ba, Q.N.; Song, R.B.; Zhou, N.P.; Pei, Z.Z.; Feng, Y.F.; Song, R.F. Revealing working hardening behavior and substructure evolutions of ultrahigh strength and enhanced wear resistance Fe-25Mn-7Al-1C steel treated by explosion processing. *J. Mater. Sci.* **2020**, *55*, 1256–1268. [[CrossRef](#)]
125. Lee, J.; Park, S.; Kim, H.; Park, S.-J.; Lee, K.; Kim, M.-Y.; Madakashira, P.P.; Han, H.N. Simulation of  $\kappa$ -Carbide Precipitation Kinetics in Aged Low-Density Fe-Mn-Al-C Steels and Its Effects on Strengthening. *Met. Mater. Int.* **2018**, *24*, 702–710. [[CrossRef](#)]
126. Feng, Y.F.; Song, R.B.; Peng, S.G.; Pei, Z.Z.; Song, R.F. Microstructures and Impact Wear Behavior of Al-Alloyed High-Mn Austenitic Cast Steel after Aging Treatment. *J. Mater. Eng. Perform.* **2019**, *28*, 4845–4855. [[CrossRef](#)]
127. Feng, Y.F.; Song, R.B.; Liu, S.; Tan, Z.D.; Peng, S.G.; Dou, G.Y. Compression Deformation Behavior of a Fe-26Mn-7Al-1.3C Austenitic Steel after Precipitation-Hardened Treatment. *Steel Res. Int.* **2019**, *90*, 1800571. [[CrossRef](#)]

128. Ren, P.; Chen, X.P.; Cao, Z.X.; Mei, L.; Li, W.J.; Cao, W.Q.; Liu, Q. Synergistic strengthening effect induced ultrahigh yield strength in lightweight Fe 30Mn 11Al-1.2C steel. *Mater. Sci. Eng.* **2019**, *752*, 160–166. [[CrossRef](#)]
129. Chao, C.Y.; Liu, C.H. Effects of Mn contents on the microstructure and mechanical properties of the Fe-10Al-xMn-1.0C alloy. *Mater. Trans.* **2002**, *43*, 2635–2642. [[CrossRef](#)]
130. Hwang, S.W.; Ji, J.N.; Park, K.T. Effects of Al addition on high strain rate deformation of fully austenitic high Mn steels. *Mater. Sci. Eng.* **2011**, *528*, 7267–7275. [[CrossRef](#)]
131. Kim, S.H.; Kim, H.; Kim, N.J. Brittle intermetallic compound makes ultrastrong low-density steel with large ductility. *Nature* **2015**, *518*, 77–79. [[CrossRef](#)] [[PubMed](#)]
132. Wang, W.J.; Man, T.H.; Zhang, M.; Wang, Y.; Dong, H.  $\delta$ -ferrite dynamic recrystallization behavior during thermal deformation in Fe-32Mn-11Al-0.9C low density steel. *J. Mater. Res. Technol.* **2022**, *18*, 1345–1357. [[CrossRef](#)]
133. Xu, L.X.; Wu, H.B. Microstructural evolution and mechanical property optimization under solution treatment of an ultra-low carbon Fe-Mn-Al duplex steel. *Mater. Sci. Eng.* **2018**, *738*, 163–173. [[CrossRef](#)]
134. Xu, L.X.; Wu, H.B.; Xie, B.S. An improved constitutive model for high-temperature flow behaviour of the Fe-Mn-Al duplex steel. *Mater. Sci. Technol.* **2018**, *34*, 229–241. [[CrossRef](#)]
135. Yao, M.  $\kappa$ -Carbide in a High-Mn Light-Weight Steel: Precipitation, off-Stoichiometry and Deformation. Ph.D. Dissertation, Universitätsbibliothek der RWTH Aachen, Aachen, Germany, 2017.
136. Yao, M.J.; Dey, P.; Seol, J.B.; Choi, P.; Raabe, D. Combined atom probe tomography and density functional theory investigation of the Al off-stoichiometry of  $\kappa$ -carbides in an austenitic Fe-Mn-Al-C low density steel. *Acta Mater.* **2016**, *106*, 229–238. [[CrossRef](#)]
137. Sato, K.; Tagawa, K.; Inoue, Y. Spinodal decomposition and mechanical properties of an austenitic Fe-30wt.%Mn-9wt.%Al-0.9wt.%C alloy. *Mater. Sci. Eng.* **1989**, *111*, 45–50. [[CrossRef](#)]
138. Cheng, W.-C.; Cheng, C.-Y.; Hsu, C.-W.; Laughlin, D.E. Phase transformation of the L12 phase to kappa-carbide after spinodal decomposition and ordering in an Fe-C-Mn-Al austenitic steel. *Mater. Sci. Eng.* **2015**, *642*, 128–135. [[CrossRef](#)]
139. Han, K.H.; Yoon, J.C.; Choo, W.K. TEM evidence of modulated structure in Fe-Mn-Al-C austenitic alloys. *Scr. Metall.* **1986**, *20*, 33–36. [[CrossRef](#)]
140. Sato, K.; Tagawa, K.; Inoue, Y. Age hardening of an Fe-30Mn-9Al-0.9C alloy by spinodal decomposition. *Scr. Metall.* **1988**, *22*, 899–902. [[CrossRef](#)]
141. Wang, Z.W.; Lu, W.J.; Zhao, H.; He, J.Y.; Wang, K.; Zhou, B.C.; Ponge, D.; Raabe, D.; Li, Z.M. Formation mechanism of  $\kappa$ -carbides and deformation behavior in Si-alloyed FeMnAlC lightweight steels. *Acta Mater.* **2020**, *198*, 258–270. [[CrossRef](#)]
142. Li, Z.; Wang, Y.C.; Cheng, X.W.; Li, Z.Y.; Du, J.K.; Li, S.K. The effect of Ti-Mo-Nb on the microstructures and tensile properties of a Fe-Mn-Al-C austenitic steel. *Mater. Sci. Eng.* **2020**, *780*, 139220. [[CrossRef](#)]
143. Zhang, J.L.; Hu, C.H.; Liu, Y.X.; Yang, Y.; Ji, G.; Song, C.J.; Zhai, Q.J. Precipitation strengthening of nano-scale TiC in a duplex low-density steel under near-rapid solidification. *J. Iron Steel Res. Int.* **2021**, *28*, 1141–1148. [[CrossRef](#)]
144. Park, B.H.; Kim, C.W.; Lee, K.W.; Park, J.U.; Park, S.J.; Hong, H.U. Role of Nb Addition on Microstructural Stability and Deformation Behaviors of FeMnAlC Lightweight Steels at 400 degrees C. *Metall. Mater. Trans.* **2021**, *52*, 4191–4205. [[CrossRef](#)]
145. Han, K.H. The microstructures and mechanical properties of an austenitic Nb-bearing Fe-Mn-Al-C alloy processed by controlled rolling. *Mater. Sci. Eng.* **2000**, *279*, 1–9. [[CrossRef](#)]
146. Ma, T.; Gao, J.X.; Li, H.R.; Li, C.Q.; Zhang, H.C.; Li, Y.G. Microband-Induced Plasticity in a Nb Content Fe-28Mn-10Al-C Low Density Steel. *Metals* **2021**, *11*, 345. [[CrossRef](#)]
147. Gao, S.; Yoshimura, T.; Mao, W.Q.; Bai, Y.; Gong, W.; Park, M.H.; Shibata, A.; Adachi, H.; Sato, M.; Tsuji, N. Tensile Deformation of Ultrafine-Grained Fe-Mn-Al-Ni-C Alloy Studied by in situ Synchrotron Radiation X-ray Diffraction. *Crystals* **2020**, *10*, 1115. [[CrossRef](#)]
148. Kim, C.; Hong, H.-U.; Jang, J.H.; Lee, B.H.; Park, S.-J.; Moon, J.; Lee, C.-H. Reverse partitioning of Al from  $\kappa$ -carbide to the  $\gamma$ -matrix upon Ni addition and its strengthening effect in Fe-Mn-Al-C lightweight steel. *Mater. Sci. Eng.* **2021**, *820*, 141563. [[CrossRef](#)]
149. Zargarán, A.; Trang, T.T.T.; Park, G.; Kim, N.J.  $\kappa$ -Carbide assisted nucleation of B2: A novel pathway to develop high specific strength steels. *Acta Mater.* **2021**, *220*, 117349. [[CrossRef](#)]
150. Liu, Y.X.; Liu, M.X.; Zhang, J.L.; He, W.; Luo, Z.P.; Song, C.J.; Zhai, Q.J. Microstructure and mechanical properties of a Fe-28Mn-9Al-1.2C-(0,3,6,9)Cr austenitic low-density steel. *Mater. Sci. Eng.* **2021**, *821*, 141583. [[CrossRef](#)]
151. Yoo, J.; Jo, M.C.; Kim, D.W.; Song, H.; Koo, M.; Sohn, S.S.; Lee, S. Effects of Cu addition on resistance to hydrogen embrittlement in 1 GPa-grade duplex lightweight steels. *Acta Mater.* **2020**, *196*, 370–383. [[CrossRef](#)]
152. Liu, M.X.; Li, X.; Zhang, Y.H.; Song, C.J.; Zhai, Q.J. Multiphase precipitation and its strengthening mechanism in a V-containing austenite-based low density steel. *Intermetallics* **2021**, *134*, 107179. [[CrossRef](#)]
153. Moon, J.; Ha, H.Y.; Park, S.J.; Lee, T.H.; Jang, J.H.; Lee, C.H.; Han, H.N.; Hong, H.U. Effect of Mo and Cr additions on the microstructure, mechanical properties and pitting corrosion resistance of austenitic Fe-30Mn-10.5Al-1.1C lightweight steels. *J. Alloy Compd.* **2019**, *775*, 1136–1146. [[CrossRef](#)]
154. Zhang, G.F.; Ma, W.; Tang, Y.H.; Wang, F.; Zhang, X.Y.; Wang, Q.F.; Liu, R.P. Investigation on the microstructural evolution and mechanical properties of partially recrystallized Fe-27Mn-10Al-1.4C steel. *Mater. Sci. Eng.* **2022**, *833*, 142545. [[CrossRef](#)]
155. Kwok, T.W.J.; Rahman, K.M.; Vorontsov, V.A.; Dye, D. Strengthening  $\kappa$ -carbide steels using residual dislocation content. *Scr. Mater.* **2022**, *213*, 114626. [[CrossRef](#)]

156. Liu, M.X.; Li, X.; Zhang, Y.H.; Song, C.J.; Zhai, Q.J. Precipitation of  $\kappa$ -Carbide in a V-Containing Austenite-Based Lightweight Steel. *Metall. Mater. Trans.* **2022**, *53*, 1231–1243. [[CrossRef](#)]
157. Saha, M.; Ponnuchamy, M.B.; Sadhasivam, M.; Mahata, C.; Vijayaragavan, G.; Gururaj, K.; Suresh, K.; Chandrasekaran, N.; Prabhu, D.; Kumbhar, K.; et al. Revealing the Localization of NiAl-Type Nano-Scale B2 Precipitates Within the BCC Phase of Ni Alloyed Low-Density FeMnAlC Steel. *JOM* **2022**, *74*, 3181–3190. [[CrossRef](#)]
158. Peng, S.G.; Song, R.B.; Sun, T.; Pei, Z.Z.; Cai, C.H.; Feng, Y.F.; Tan, Z.D. Wear Behavior and Hardening Mechanism of Novel Lightweight Fe-25.1Mn-6.6Al-1.3C Steel Under Impact Abrasion Conditions. *Tribol. Lett.* **2016**, *64*, 13. [[CrossRef](#)]
159. Li, Z.; Wang, Y.C.; Cheng, X.W.; Li, Z.Y.; Gao, C.; Li, S.K. The effect of rolling and subsequent aging on microstructures and tensile properties of a Fe-Mn-Al-C austenitic steel. *Mater. Sci. Eng.* **2021**, *822*, 141683. [[CrossRef](#)]
160. Lee, S.; Kang, S.H.; Nam, J.H.; Lee, S.M.; Seol, J.B.; Lee, Y.K. Effect of Tempering on the Microstructure and Tensile Properties of a Martensitic Medium-Mn Lightweight Steel. *Metall. Mater. Trans.* **2019**, *50A*, 2655–2664. [[CrossRef](#)]
161. Byun, T.S. On the stress dependence of partial dislocation separation and deformation microstructure in austenitic stainless steels. *Acta Mater.* **2003**, *51*, 3063–3071. [[CrossRef](#)]
162. Moon, J.; Park, S.-J.; Jang, J.H.; Lee, T.-H.; Lee, C.-H.; Hong, H.-U.; Suh, D.-W.; Kim, S.H.; Han, H.N.; Lee, B.H. Atomistic investigations of  $\kappa$ -carbide precipitation in austenitic Fe-Mn-Al-C lightweight steels and the effect of Mo addition. *Scr. Mater.* **2017**, *127*, 97–101. [[CrossRef](#)]
163. Kim, K.W.; Park, S.J.; Moon, J.; Jang, J.H.; Ha, H.Y.; Lee, T.H.; Hong, H.U.; Lee, B.H.; Han, H.N.; Lee, Y.J.; et al. Characterization of microstructural evolution in austenitic Fe-Mn-Al-C lightweight steels with Cr content. *Mater. Charact.* **2020**, *170*, 110717. [[CrossRef](#)]
164. Zhang, J.L.; Liu, Y.X.; Hu, C.H.; Jiang, Y.S.; Addad, A.; Ji, G.; Song, C.J.; Zhai, Q.J. The effect of Cr content on intragranular  $\kappa$ -carbide precipitation in Fe-Mn-Al-(Cr)-C low-density steels: A multiscale investigation. *Mater. Charact.* **2022**, *186*, 111801. [[CrossRef](#)]
165. Yang, L.; Li, Z.M.; Li, X.; Zhang, Y.H.; Han, K.; Song, C.J.; Zhai, Q.J. An Enhanced Fe-28Mn-9Al-0.8C Lightweight Steel by Coprecipitation of Nanoscale Cu-Rich and  $\kappa$ -Carbide Particles. *Steel Res. Int.* **2020**, *91*, 1900665. [[CrossRef](#)]
166. Rahnama, A.; Kotadia, H.; Sridhar, S. Effect of Ni alloying on the microstructural evolution and mechanical properties of two duplex light-weight steels during different annealing temperatures: Experiment and phase-field simulation. *Acta Mater.* **2017**, *132*, 627–643. [[CrossRef](#)]
167. Kaar, S.; Krizan, D.; Schwabe, J.; Hofmann, H.; Hebesberger, T.; Commenda, C.; Samek, L. Influence of the Al and Mn content on the structure-property relationship in density reduced TRIP-assisted sheet steels. *Mater. Sci. Eng.* **2018**, *735*, 475–486. [[CrossRef](#)]
168. Wang, W.L.; An, Z.J.; Luo, S.; Zhu, M.Y. In-situ observation of peritectic solidification of Fe-Mn-Al-C steel with medium manganese. *J. Alloy Compd.* **2022**, *909*, 164750. [[CrossRef](#)]
169. Zhao, J.X.; Zhu, H.Y.; Wang, L.Q.; Song, M.M.; Li, J.L.; Xue, Z.L. Effect of CaO/Al<sub>2</sub>O<sub>3</sub> ratio on desulphurization and non-metallic inclusions in low-density steel. *Ironmak. Steelmak.* **2022**, *49*, 302–310. [[CrossRef](#)]
170. Ji, C.X.; Cui, Y.; Zeng, Z.; Tian, Z.H.; Zhao, C.L.; Zhu, G.S. Continuous Casting of High-Al Steel in Shougang Jingtang Steel Works. *J. Iron Steel Res. Int.* **2015**, *22*, 53–56. [[CrossRef](#)]
171. Li, K.W.; Zhuang, C.L.; Liu, J.H.; Shen, S.B.; Ji, Y.L.; Han, Z.B. Smelting and Casting Technologies of Fe-25Mn-3Al-3Si Twinning Induced Plasticity Steel for Automobiles. *J. Iron Steel Res. Int.* **2015**, *22*, 75–79. [[CrossRef](#)]
172. Chen, Z.; Liu, M.X.; Zhang, J.K.; Yang, L.; Zhang, Y.H.; Song, C.J.; Zhai, Q.J. Effect of annealing treatment on microstructures and properties of austenite-based Fe-28Mn-9Al-0.8C lightweight steel with addition of Cu. *China Foundry* **2021**, *18*, 207–216. [[CrossRef](#)]
173. Zhang, J.L.; Hu, C.H.; Zhang, Y.H.; Li, J.H.; Song, C.J.; Zhai, Q.J. Microstructures, mechanical properties and deformation of near-rapidly solidified low-density Fe-20Mn-9Al-1.2C-xCr steels. *Mater. Des.* **2020**, *186*, 108307. [[CrossRef](#)]
174. Leonhardt, M.; Loser, W.; Lindenkreuz, H.G. Solidification kinetics and phase formation of undercooled eutectic Ni-Nb melts. *Acta Mater.* **1999**, *47*, 2961–2968. [[CrossRef](#)]
175. Li, Y.P.; Song, R.B.; Wen, E.D.; Yang, F.Q. Hot Deformation and Dynamic Recrystallization Behavior of Austenite-Based Low-Density Fe-Mn-Al-C Steel. *Acta Metall. Sin.-Engl. Lett.* **2016**, *29*, 441–449. [[CrossRef](#)]
176. Mohamadizadeh, A.; Zarei-Hanzaki, A.; Abedi, H.R.; Mehtonen, S.; Porter, D. Hot deformation characterization of duplex low-density steel through 3D processing map development. *Mater. Charact.* **2015**, *107*, 293–301. [[CrossRef](#)]
177. Abedi, H.R.; Hanzaki, A.Z.; Liu, Z.; Xin, R.; Haghdadi, N.; Hodgson, P.D. Continuous dynamic recrystallization in low density steel. *Mater. Des.* **2017**, *114*, 55–64. [[CrossRef](#)]
178. Wu, Z.Q.; Tang, Y.B.; Chen, W.; Lu, L.W.; Li, E.; Li, Z.C.; Ding, H. Exploring the influence of Al content on the hot deformation behavior of FeMn-Al-C steels through 3D processing map. *Vacuum* **2019**, *159*, 447–455. [[CrossRef](#)]
179. Pierce, D.T.; Field, D.M.; Limmer, K.R.; Muth, T.; Sebeck, K.M. Hot deformation behavior of an industrially cast large grained low density austenitic steel. *Mater. Sci. Eng.* **2021**, *825*, 141785. [[CrossRef](#)]
180. Zambrano, O.A.; Valdes, J.; Aguilar, Y.; Coronado, J.J.; Rodriguez, S.A.; Loge, R.E. Hot deformation of a Fe-Mn-Al-C steel susceptible of kappa-carbide precipitation. *Mater. Sci. Eng.* **2017**, *689*, 269–285. [[CrossRef](#)]

181. Liu, D.G.; Ding, H.; Hu, X.; Han, D.; Cai, M.H. Dynamic recrystallization and precipitation behaviors during hot deformation of a  $\kappa$ -carbide-bearing multiphase Fe-11Mn-10Al-0.9C lightweight steel. *Mater. Sci. Eng.* **2020**, *772*, 138682. [[CrossRef](#)]
182. Liu, D.G.; Ding, H.; Cai, M.H.; Han, D. Hot Deformation Behavior and Processing Map of a Fe-11Mn-10Al-0.9C Duplex Low-Density Steel Susceptible to kappa-Carbides. *J. Mater. Eng. Perform.* **2019**, *28*, 5116–5126. [[CrossRef](#)]
183. Mozumder, Y.H.; Babu, K.A.; Saha, R.; Sarma, V.S.; Mandal, S. Dynamic microstructural evolution and recrystallization mechanism during hot deformation of intermetallic-hardened duplex lightweight steel. *Mater. Sci. Eng.* **2020**, *788*, 139613. [[CrossRef](#)]